

1 **Title: The spike gene is a major determinant for the SARS-CoV-2 Omicron-BA.1**
2 **phenotype**

3 **Short title:** SARS-CoV-2 spike drives Omicron phenotype

4 **Authors:** Tuba Barut^{1,2†}, Nico Joel Halwe^{3†}, Adriano Taddeo^{1,2†}, Jenna N. Kelly^{1,2,4,5†},
5 Jacob Schön³, Nadine Ebert^{1,2}, Lorenz Ulrich³, Christelle Devisme^{1,2}, Silvio Steiner^{1,2}, Bettina
6 Salome Trüeb^{1,2}, Bernd Hoffmann³, Inês Berenguer Veiga^{1,2}, Nathan Georges François
7 Leborgne^{1,2}, Etori Aguiar Moreira^{1,2}, Angele Breithaupt⁶, Claudia Wylezich³, Dirk Höper³,
8 Kerstin Wernike³, Aurélie Godel^{1,2}, Lisa Thomann^{1,2}, Vera Flück^{1,2}, Hanspeter Stalder^{1,2},
9 Melanie Brügger^{1,2}, Blandina I. Oliveira Esteves^{1,2}, Beatrice Zumkehr^{1,2}, Guillaume
10 Beilleau^{1,2,7}, Annika Kratzel^{1,2}, Kimberly Schmied^{1,2}, Sarah Ochsenbein^{1,2}, Reto M. Lang^{1,2,7},
11 Manon Wider⁸, Carlos Machahua^{9,10}, Patrick Dorn^{11,12}, Thomas M. Marti^{11,12}, Manuela
12 Funke-Chambour^{9,10}, Andri Rauch^{4,13}, Marek Widera¹⁴, Sandra Ciesek¹⁴, Ronald Dijkman^{4,5,8},
13 Donata Hoffmann³, Marco P. Alves^{1,2,4,†*}, Charaf Benarafa^{1,2,4,†*}, Martin Beer^{3,5,†*}, Volker
14 Thiel^{1,2,4,5,†*}

15 **Affiliations:**

16 ¹Institute of Virology and Immunology, Bern and Mittelhäusern, Switzerland

17 ²Department of Infectious Diseases and Pathobiology, Vetsuisse Faculty, University of Bern,
18 Bern, Switzerland

19 ³Institute of Diagnostic Virology, Friedrich-Loeffler-Institut, Greifswald-Insel Riems,
20 Germany

21 ⁴Multidisciplinary Center for Infectious Diseases, University of Bern, Bern, Switzerland

22 ⁵European Virus Bioinformatics Center, Jena, Germany

23 ⁶Department of Experimental Animal Facilities and Biorisk Management, Friedrich-Loeffler-
24 Institut, Greifswald-Insel Riems, Germany

25 ⁷Graduate School for Cellular and Biomedical Sciences, University of Bern, Bern,
26 Switzerland

27 ⁸Institute for Infectious Diseases, University of Bern, Bern, Switzerland

28 ⁹Department of Pulmonary Medicine, Inselspital, Bern University Hospital, University of
29 Bern, Bern, Switzerland

30 ¹⁰Department for Pulmonary Medicine, BioMedical Research, University of Bern, Bern,
31 Switzerland

32 ¹¹Division of General Thoracic Surgery, Inselspital, Bern University Hospital, University of
33 Bern, Bern, Switzerland

34 ¹²Department for BioMedical Research, Inselspital, Bern University Hospital, University of
35 Bern, Switzerland

36 ¹³Department of Infectious Diseases, Inselspital, Bern University Hospital, University of
37 Bern, Switzerland

38 ¹⁴Institute of Medical Virology, University Hospital Frankfurt, Goethe University, Frankfurt
39 am Main, Germany

40

41 [†]These authors contributed equally to this work.

42 [‡]These authors jointly lead this work.

43

44 *Corresponding authors.

45 Volker Thiel; e-mail: volker.thiel@vetsuisse.unibe.ch; phone: +41-31-6312413

46 Charaf Benarafa; e-mail: charaf.benarafa@vetsuisse.unibe.ch; phone: +41-58-4699246

47 Martin Beer; e-mail: martin.beer@fli.de; phone: +49-38-35171200

48 Marco P. Alves; e-mail: marco.alves@vetsuisse.unibe.ch; phone: +41 31 684 2483

49

50 Abstract: 211 words ; main text : 4023 words.

51 **Abstract**

52 Variant of concern (VOC) Omicron-BA1 has achieved global predominance in early 2022.
53 Therefore, surveillance and comprehensive characterization of Omicron-BA.1 in advanced
54 primary cell culture systems and multiple animal models is urgently needed. Here, we
55 characterized Omicron-BA.1 and recombinant Omicron-BA.1 spike gene mutants in
56 comparison with VOC Delta in well-differentiated primary human nasal and bronchial
57 epithelial cells *in vitro*, followed by *in vivo* fitness characterization in naïve hamsters, ferrets
58 and hACE2-expressing mice, and in immunized hACE2-mice. We demonstrate a spike-
59 mediated enhancement of early replication of Omicron-BA.1 in nasal epithelial cultures, but
60 limited replication in bronchial epithelial cultures. In Syrian hamsters, Delta showed
61 dominance over Omicron-BA.1 and in ferrets, Omicron-BA.1 infection was abortive. In mice
62 expressing the authentic hACE2-receptor, Delta and a Delta spike clone also showed
63 dominance over Omicron-BA.1 and an Omicron-BA.1 spike clone, respectively. Interestingly,
64 in naïve K18-hACE2 mice, we observed Delta spike-mediated increased replication and
65 pathogenicity and Omicron-BA.1 spike-mediated reduced replication and pathogenicity,
66 suggesting that the spike gene is a major determinant of both Delta and Omicron-BA.1
67 replication and pathogenicity. Finally, the Omicron-BA.1 spike clone was less well controlled
68 by mRNA-vaccination in K18-hACE2-mice and became more competitive compared to the
69 progenitor and Delta spike clones, suggesting that spike gene-mediated immune evasion is
70 another important factor that led to Omicron-BA.1 dominance.

71 **Introduction**

72 On a global scale, SARS-CoV-2 evolution can be tracked by identifying independently
73 emerging variants of concern (VOCs), with VOC Alpha, Delta, and Omicron dominating
74 successively. Delta carries two deterministic mutations potentially leading to increased
75 fitness: L452R, conferring immune escape¹, and P681R, conferring enhanced transmission².
76 Omicron-BA.1 holds in total up to 50 mutations, with 34 located in the spike (S) gene, 15 of
77 which are within the receptor-binding domain (RBD)³. A defining Omicron-BA.1 mutation is
78 ins214EPE, a three-amino acid insertion, whose role for viral fitness is still unknown.
79 However, this VOC is characterized by its remarkable ability to evade neutralizing antibodies
80 up to 40 times more efficiently than the ancestral SARS-CoV-2 and pre-Omicron variants^{4,5}.
81 In January 2022, the Omicron-BA.1 lineage became predominant in most countries
82 worldwide⁶ and has since then largely been replaced by the related Omicron-BA.2. It remains
83 elusive if the rapid spread of Omicron-BA.1 and the replacement of Delta is due to increased
84 fitness and transmission, or if it is mainly based on its immune escape ability allowing
85 efficient infection and transmission chains among double-vaccinated and even boosted
86 individuals. The genetic determinants for the Omicron-BA.1 phenotype also remain largely
87 undefined. With high prevalence of concurrent VOCs and reports of recombination events in
88 communities⁷, it is crucial to characterize differences in viral fitness and immune escape of
89 emerging and prevailing VOCs in advanced cell culture and animal models⁸.
90 While mouse models expressing human angiotensin-converting enzyme 2 (hACE2) and
91 Syrian hamsters are highly susceptible for SARS-CoV-2 and show signs of severe disease,
92 ferrets display subclinical infection despite efficient viral replication of SARS-CoV-2 in the
93 upper respiratory tract (URT)^{9,10}. An experimental setup applying competitive infection and
94 transmission experiments in different species has become a gold-standard method to
95 investigate VOC fitness⁹⁻¹². With this experimental approach, viral fitness advantages or

96 disadvantages of SARS-CoV-2 VOCs can be analyzed in direct comparison at the nucleotide
97 and at variant level.

98 Here, we demonstrate a dominance of Delta over Alpha in ferrets, whereas in Syrian
99 hamsters, Alpha dominated Delta. Moreover, we demonstrate that the advent of the Omicron
100 VOC in the evolution of SARS-CoV-2 is a radical change from the incremental improvements
101 in fitness observed in previous pandemic VOCs. Using a comprehensive experimental VOC
102 competition approach against Delta, we demonstrate that the Omicron-BA.1 phenotype is
103 characterized by (i) a reduced replication and transmission fitness in Syrian hamsters, (ii) a
104 failure to replicate in ferrets, (iii) an accelerated growth in human epithelial cell cultures
105 mimicking the upper respiratory tract, (iv) a reduced replication in lung explants and primary
106 human bronchial epithelial cultures, resembling conditions of the human lower respiratory
107 tract, (v) a reduced replication fitness in naïve human ACE2 (hACE2) expressing knock-in
108 (hACE2-KI) and transgenic (K18-hACE2) mice, and (vi) evidence of immune evasion in
109 mRNA-vaccinated K18-hACE2 mice. Importantly, we show that the spike gene is a major
110 determinant in the Omicron-BA.1 phenotype based on experiments *in vitro* and *in vivo* using
111 recombinant SARS-CoV-2 clones differing only by the expression of the spike protein of the
112 respective VOCs.

113

114 **Results**

115 **Omicron-BA.1 spike enhances viral replication in the nasal but not bronchial epithelium**

116 In order to assess the phenotypes of the VOCs Delta and Omicron-BA.1 and to evaluate the
117 contribution of changes within the spike protein, we constructed a set of recombinant SARS-
118 CoV-2 clones containing defined mutations in the spike gene (Fig. 1a). All constructs have an
119 isogenic background based on the Wuhan-Hu-1 sequence and differ only in the spike gene,
120 which was modified to contain lineage-defining spike gene mutations of the VOC Delta

121 (SARS-CoV-2^{S-Delta}), VOC Omicron-BA.1 (SARS-CoV-2^{S-Omicron}), mutations of the Omicron-
122 BA.1 spike N-terminal domain (NTD; SARS-CoV-2^{NTD-Omicron}), mutations of the Omicron-
123 BA.1 spike receptor-binding domain (RBD; SARS-CoV-2^{RBD-Omicron}), or the mutations at and
124 near the Omicron-BA.1 spike cleavage site region (CS; SARS-CoV-2^{CS-Omicron}). All
125 recombinant viruses replicated but showed noticeable differences in plaque sizes (Fig. 1b).
126 Compared to the index virus SARS-CoV-2^{D614G} (recombinant SARS-CoV-2 based on Wuhan-
127 Hu-1 with the spike change D614G¹¹, the Delta isolate showed smaller plaques, while
128 plaques of SARS-CoV-2^{S-Delta} were considerably larger. Interestingly, SARS-CoV-2^{S-Omicron}
129 displayed small plaques that were indistinguishable from the isolate of Omicron-BA.1
130 (EPI_ISL_7062525), but plaques of Omicron-BA.1 spike subdomain clones (SARS-CoV-
131 2^{NTD-Omicron}, SARS-CoV-2^{CS-Omicron}, SARS-CoV-2^{RBD-Omicron}) differed in size (Fig. 1b),
132 indicating possible phenotypic differences of the Omicron-BA.1 spike subdomain clones
133 compared to the Omicron-BA.1 isolate and the full-length Omicron-BA.1 spike clone.

134 Next, we infected well-differentiated primary human nasal and bronchial epithelial cell
135 cultures (hNECs and hBECs, respectively) at 33°C for hNECs and at 37°C for hBECs (Fig.
136 1c,d). Delta and the corresponding spike construct SARS-CoV-2^{S-Delta} replicated with similar
137 kinetics as wild-type SARS-CoV-2^{D614G} on both hNECs and hBECs, with SARS-CoV-2^{S-Delta}
138 reaching the highest apical titers at 72-96 hours post-infection (hpi) (Fig. 1c). Strikingly,
139 replication kinetics of Omicron-BA.1 and the corresponding spike clone SARS-CoV-2^{S-Omicron}
140 displayed accelerated growth within the first 48 hpi on hNECs. In contrast, on hBECs,
141 Omicron-BA.1 and SARS-CoV-2^{S-Omicron} did not show this early accelerated growth, and
142 moreover, showed significantly reduced viral titers at later time points. This phenotype was
143 confirmed by competition assays on hNECs and hBECs using various combinations of viruses
144 in the inoculum (Fig. 1e,f; Extended Data Fig. 1). On hNECs, the Omicron-BA.1 isolate and
145 the corresponding SARS-CoV-2^{S-Omicron} outcompeted SARS-CoV-2^{D614G}, the Delta isolate,

146 and SARS-CoV-2^{S-Delta} (Fig. 1d). In contrast, the dominance of the Omicron-BA.1 isolate, and
147 SARS-CoV-2^{S-Omicron} was reduced in hBECs (Fig. 1d). Finally, SARS-CoV-2^{S-Delta} was
148 dominant over SARS-CoV-2^{S-Omicron} in an ex vivo distal lung explant system (Fig. 1g)
149 Collectively, studies *in vitro* under conditions mimicking the native human upper respiratory
150 tract epithelium (URT; hNECs at 33°C) remarkably demonstrate that the Omicron-BA.1 spike
151 gene (Omicron-BA.1 isolate and SARS-CoV-2^{S-Omicron}) confers accelerated virus replication
152 and increased replicative fitness compared to pre-Omicron spike genes (SARS-CoV-2^{D614G}, a
153 Delta isolate, and SARS-CoV-2^{S-Delta}). In contrast, under conditions resembling the human
154 lower respiratory tract epithelium (LRT; hBECs, 37°C; lung explants), the Omicron-BA.1
155 spike gene confers reduced virus replication.

156

157 **Replicative fitness and transmission of VOCs Alpha, Delta, and Omicron in Syrian
158 hamsters**

159 To evaluate individual VOC fitness advantages in direct competition with the precursing
160 VOC, we then turned to animal models with natural susceptibility towards SARS-CoV-2:
161 ferrets and Syrian hamsters. Donor animals were simultaneously co-inoculated with two
162 VOCs at iso-titer and transmission to contact animals was investigated (Extended Data Fig.
163 2a,b).

164 We investigated fitness of the VOC Delta in competition with Alpha after intranasal co-
165 inoculation of $10^{4.625}$ TCID₅₀ of an Alpha-Delta mixture at a 1.95:1 ratio (Extended Data Fig.
166 2a, 5). For all donor and contact hamsters, Alpha showed complete dominance in nasal
167 washings and respiratory tissues (Extended Data Fig. 5, 8). The animals showed signs of
168 severe disease and 10 of 12 contact hamsters reached the humane endpoint, (defined by a 20%
169 loss of the initial body weight) (Extended Data Fig. 3a,c, 5). While Alpha was clearly

170 dominant in all animals, sera equally neutralized Alpha and Delta VOCs (VNT₁₀₀) (Extended
171 Data Fig. 7a).

172 We also tested Delta vs Omicron-BA.1 (total 10^{4.5} TCID₅₀ at a 1:2.16 ratio) in hamsters (Fig.
173 2a, Extended Data Fig. 2a). Upon inoculation or contact, all animals lost body weight,
174 however, only one animal was euthanized after reaching the humane endpoint for body
175 weight loss (Fig. 2a, Extended Data Fig. 3b,d). Although starting with a clear advantage for
176 Omicron-BA.1 in the inoculum, Delta was immediately prevalent in nasal washings of donor
177 hamsters with up to 10⁸ genome copies per mL (GE/mL) (Fig. 2a). Remarkably, despite high
178 genome loads of Delta, Omicron-BA.1 still replicated to 10⁷ GE/mL (Fig. 2a). Nevertheless,
179 Delta was preferentially transmitted as seen in both nasal washings and organ samples of
180 contact animals (Fig. 2a, Extended Data Fig. 4). In tissues of donor animals at 4 dpi, mainly
181 Delta was found in the upper (URT) and lower respiratory tract (LRT) (Fig. 2b); with highest
182 Delta loads in the nasal concha (10⁸ GE/mL). However, Omicron-BA.1 was still present in the
183 URT of each donor animal (up to 10⁷ GE/mL) (Fig. 2b). Consequently, the antibody response
184 was mainly directed against Delta with neutralization up to a serum dilution of 1:1024, while
185 Omicron-BA.1 was only barely neutralized (Fig. 2d). Together, we show that the Syrian
186 hamster is highly susceptible also for the SARS-CoV-2 VOCs Alpha, Delta, and Omicron-
187 BA.1. However, the Alpha VOC seems to be best replicating and transmitting in the Syrian
188 hamster model associated with the highest fatality rates.

189

190 **Omicron-BA.1 fails to induce productive infection in ferrets**

191 For further characterization of the different VOCs, we also inoculated ferrets, which are
192 known to mirror human respiratory disease. First, animals were inoculated with a Delta isolate
193 (Extended Data Fig. 2c). All animals remained clinically healthy and did not lose body weight
194 (Extended Data Fig. 3e). Viral shedding was confirmed for all donor animals by nasal

195 washing for up to 10 days, with highest viral genome loads of up to more than 10^7 GE/mL at
196 5 and 6 dpi (Fig. 2f). Two out of three contact animals were infected by 6 days post contact
197 (dpc) and viral loads in contacts reached up to 10^8 GE/mL (Fig. 2f). These results were also
198 confirmed by serology (Fig. 2f).

199 Next, ferrets were co-inoculated with VOCs Alpha and Delta (1.33:1 ratio, 10^5 TCID₅₀ in
200 total) (Extended Data Fig. 2b, 6). All ferrets remained clinically healthy throughout the
201 animal experiment and did not lose body weight (Extended Data Fig. 3g). Within 3 days,
202 Delta fully outcompeted Alpha in both replication and transmission (Extended Data Fig. 6),
203 which is in line with the epidemiological situation observed in humans. These observations
204 were further supported by the matching serological data (Extended Data Fig. 7b).

205 We finally investigated competition of Delta and Omicron-BA.1 in the ferret model by
206 inoculating a $10^{4.75}$ TCID₅₀ Delta-Omicron mixture (1:1.43 ratio) (Fig. 2c, Extended Data Fig.
207 2B). All ferrets remained clinically healthy throughout the animal experiment and did not lose
208 body weight (Extended Data Fig. 3h). Astonishingly, only Delta was detected in all nasal
209 washings of the donor ferrets, starting at 1 dpi at levels of up to 10^7 GE/mL (Fig. 2c). In
210 addition, 5 out of 6 contact ferrets showed shedding of Delta (highest loads: 10^7 GE/mL),
211 starting at 2 dpc (Fig. 2c). The shedding interval lasted up to 12 days in the donor ferrets (Fig.
212 2c). Surprisingly, Omicron-BA.1 was not detected in any donor, hence only Delta was
213 transmitted to contact ferrets (Fig. 2c). These results indicate a severe block of Omicron-BA.1
214 infection in ferrets. To confirm the unexpected observation, we inoculated ferrets with
215 Omicron-BA.1 only with in total $10^{5.125}$ TCID₅₀ (Extended Data Fig. 2c). All ferrets
216 remained clinically healthy throughout the study with no marked body weight changes
217 (Extended Data Fig. 3f). Again, we detected neither shedding of Omicron-BA.1 in nasal
218 washings, nor vRNA in the URT or LRT of ferrets euthanized at 6dpi (Fig. 2f). Serological
219 analysis confirmed the RT-qPCR results by revealing lack of seroconversion at 21 dpi (Fig.

220 2f). Successful back-titration of the Omicron-BA.1 inocula for each experiment, whole-
221 genome sequence confirmation by high-throughput sequencing and using the same virus stock
222 for both the hamster and the ferret experiments, strongly suggest a complete replication block
223 of VOC Omicron-BA.1 in ferrets. Therefore, the Delta variant seems to exhibit the top-level
224 fitness in ferrets, and the vast changes in the Omicron-BA.1 sequence might be at the cost of
225 broad host spectrum.

226

227 **Delta spike mutations drive enhanced fitness in humanized mice**

228 To mitigate the impact of mismatched interactions between non-human ACE2 and the
229 Omicron-BA.1 spike/RBD, knock-in mice expressing only human ACE2 (hACE2-KI) were
230 inoculated intranasally with $10^{4.3}$ TCID₅₀/mouse of Omicron-BA.1 or Delta. Infection with
231 Delta only caused body weight loss at 4dpi. Higher virus loads and titers in the URT, LRT,
232 and olfactory bulb were found in mice inoculated with Delta compared to Omicron-BA.1
233 (Fig. 3a-c, Extended Data Fig. 9a). Higher virus loads in hACE2-KI mice infected with Delta
234 were associated with a higher pathological score in the lungs, which showed multifocal,
235 peribronchiolar inflammatory cuffs (Fig. 3d,e, Supplementary Information Table 1). In a
236 competition setting, Delta also dominated over Omicron-BA.1 in the URT and LRT (Fig. 3f,
237 Extended Data Fig. 9b). To determine the importance of the spike mutations, hACE2-KI mice
238 were inoculated with an equivalent mixture of recombinant clones only differing by the spike
239 sequence, SARS-CoV-2^{S-Delta} and SARS-CoV-2^{S-Omicron}. As for the VOC isolates, SARS-
240 CoV-2^{S-Delta} fully dominated over SARS-CoV-2^{S-Omicron} in the URT and LRT of hACE2-KI
241 mice indicating that the spike is of major importance for the phenotype of both VOCs and that
242 spike mutations do not provide an advantage to Omicron-BA.1 over Delta in a humanized
243 mouse model (Fig. 3g). These findings suggest that the intrinsic replicative properties of

244 Omicron-BA.1 are unlikely the decisive factor for the observed replacement of Delta by
245 Omicron-BA.1 in the human population.

246

247 **Omicron-BA.1 spike confers immune escape and reduced pathogenicity**

248 Next, we investigated the impact of prior SARS-CoV-2-specific mRNA vaccination on the
249 replicative fitness of Omicron-BA.1 and Delta (Fig. 4a). Since current mRNA vaccines use
250 the spike as the sole viral antigen, we focused on the impact of the spike gene on immune
251 evasion and replication. Further, to exclude any influence of mutations outside the spike genes
252 of the Delta and the Omicron-BA.1 VOC on replication, immune evasion, or pathogenicity,
253 we used the isogenic viruses SARS-CoV-2^{S-Delta} and SARS-CoV-2^{S-Omicron} that differ only in
254 their spike gene for infection of vaccinated and naïve mice. Transgenic K18-hACE2 were
255 immunized (1 µg of Spikevax, Moderna) once and had detectable titers of neutralizing
256 antibodies to the index virus SARS-CoV-2^{D614G} one week prior to infection compared to the
257 control groups (Fig. 4a; Extended Data Fig. 10a). Naïve and immunized mice were infected
258 intranasally with 10⁴ TCID50/mouse of SARS-CoV-2^{S-Delta}, SARS-CoV-2^{S-Omicron}, or SARS-
259 CoV-2^{D614G}.

260 Interestingly, only unvaccinated mice inoculated with SARS-CoV-2^{S-Delta}, or SARS-CoV-
261 2^{D614G} showed reduction in body weight at 6 dpi, while unvaccinated mice challenged with
262 SARS-CoV-2^{S-Omicron} and all vaccinated mice, regardless of the challenge virus, did not lose
263 body weight (Fig. 4b). Accordingly, clinical scores were highest for unvaccinated mice
264 infected with SARS-CoV-2^{S-Delta} (Extended Data Fig. 10b). Viral RNA loads in
265 oropharyngeal swabs and several organs were mostly lower for SARS-CoV-2^{S-Omicron}-infected
266 mice and remained high for SARS-CoV-2^{S-Delta} in the nasal cavity (Fig. 4c). Nevertheless,
267 viral RNA loads were in most cases reduced at 6 dpi in vaccinated mice, although, as
268 expected, reduction was less pronounced in SARS-CoV-2^{S-Delta}- and SARS-CoV-2^{S-Omicron}-

269 infected mice (Fig. 4c). Strikingly, the detection of infectious virus in the nose, lung and brain
270 of infected naïve and vaccinated mice perfectly illustrated the effect of vaccination and
271 phenotypic differences between SARS-CoV-2^{D614G}, SARS-CoV-2^{S-Delta} and SARS-CoV-2^{S-}
272 ^{Omicron} (Fig. 4d). Infectious wild-type SARS-CoV-2^{D614G} is detected in unvaccinated mice in
273 the nose and lung and later at 6 dpi at lower levels also in the brain. However, mRNA
274 immunization efficiently restricted SARS-CoV-2^{D614G} replication, as infectious virus was only
275 detectable at 2 dpi in the nose and not in any other tissue. SARS-CoV-2^{S-Delta} titers in
276 unvaccinated mice were comparable to SARS-CoV-2^{D614G} titers in the nose, while we
277 observed higher titers in the lung and particularly in the brain (Fig. 4d, Extended Data Fig.
278 10d,e). As expected, SARS-CoV-2^{S-Delta} showed some degree of immune escape as infectious
279 virus was readily detectable at 2 dpi in the nose and lung, but eventually was cleared at 6 dpi
280 in vaccinated mice (Fig. 4d). Finally, we detected less infectious virus of SARS-CoV-2^{S-}
281 ^{Omicron} compared to SARS-CoV-2^{D614G} and SARS-CoV-2^{S-Delta} in the nose, lung and brain of
282 unvaccinated mice, suggesting that the Omicron-BA.1 spike gene confers a less virulent
283 phenotype than the 614G and the Delta spike gene (Fig. 4d, Extended Data Fig. 10d,e).
284 Moreover, the Omicron-BA.1 spike gene conferred the largest degree of immune evasion,
285 since infectious titers were comparable between vaccinated and unvaccinated mice in the nose
286 at 2 and 6 dpi and in the lung at 2 dpi. However, no infectious virus was detected in the brains
287 of vaccinated mice, and titers in the lungs were reduced compared to unvaccinated mice at 6
288 dpi, suggesting that the mRNA vaccine is still of advantage to combat SARS-CoV-2^{S-Omicron}
289 infection in the LRT and systemic dissemination (Fig. 4d, Extended Data Fig. 10d,e). The
290 different virus phenotypes and vaccine efficiencies are corroborated by the pathological
291 findings (Fig. 4e, Extended Data Fig. 10c; Supplementary Information Table 2). Unvaccinated
292 mice infected with SARS-CoV-2^{S-Delta} displayed severe interstitial lymphohistiocytic
293 pneumonia with concurrent vascular inflammation and widespread nucleocapsid antigen
294 detection in the immunohistochemical (IHC) analysis starting already at 2 dpi, while infection

295 with SARS-CoV-2^{D614G} resulted in similarly severe pathological findings only at 6 dpi. In
296 contrast, unvaccinated mice that were infected with SARS-CoV-2^{S-Omicron} displayed milder
297 histopathological lung lesions and less nucleocapsid antigen was detected by IHC analysis. In
298 agreement with the observed reduced virus titers in the lungs of vaccinated mice, we observed
299 milder lung histopathological lesions and almost no nucleocapsid antigen IHC detection in
300 vaccinated mice with any of the viruses when compared to lungs of unvaccinated mice.

301 Collectively, these findings demonstrate the major impact of the Delta and Omicron-BA.1
302 spike genes on virus replication, immune evasion, and pathogenicity. Compared to the
303 progenitor D614G spike gene, the Delta spike gene confers increased replication,
304 pathogenicity, and immune escape. The Omicron-BA.1 spike gene is conferring the greatest
305 degree of immune evasion, compared to the wild-type D614G spike and the Delta spike
306 genes, resulting in comparable or even increased detection of infectious SARS-CoV-2^{S-Omicron}
307 compared to SARS-CoV-2^{D614G} and SARS-CoV-2^{S-Delta}, in several tissues and organs of
308 vaccinated mice. Importantly, the Omicron-BA.1 spike gene also confers reduced
309 pathogenicity, as seen in unvaccinated mice (Fig. 4b,e), suggesting that the Omicron-BA.1
310 spike is a major determinant of the observed milder disease in humans.

311

312 **Discussion**

313 The appearance of Omicron-BA.1 in the human population exemplified a remarkable jump in
314 SARS-CoV-2 evolution. Omicron-BA.1 has acquired up to 50 mutations of which at least 34
315 are located within the spike gene³. Particularly, the NTD and RBD harbor many mutations
316 that have not been seen in previous SARS-CoV-2 variants, suggesting substantial changes in
317 spike antigenicity, receptor binding, and possibly other spike functions. Accordingly, the
318 current experimental systems to assess phenotypic changes of SARS-CoV-2 require a revision
319 regarding the extent to which they truly reflect epidemiological and clinical observations in

320 humans. We and others previously showed that the Syrian hamster is a highly susceptible
321 animal model for several SARS-CoV-2 variants and showed a great efficiency in replication
322 and transmission^{9,10,13}. Nevertheless, we show here that competitive infection and
323 transmission experiments in the hamster model no longer reflect the human epidemiological
324 situation. While in humans, Omicron-BA.1 rapidly became the prevailing variant over Delta,
325 which afore outcompeted Alpha, we observed that in competitive infection experiments in the
326 hamster model the exact opposite order of variants is dominant. Certainly, these differential
327 observations hint to an adaptation of SARS-CoV-2 variants to the human host. Our data show
328 that Alpha is massively replicating and dominantly transmitted with severe clinical features in
329 the hamster model. Moreover, replicative fitness of Delta and Omicron-BA.1 decreased
330 sequentially in direct competition with the respective earlier predominant variant in the
331 human population^{14,15}. These observations are in line with the high degree of mortality (83 %
332 mortality) in the Delta vs Alpha compared to the Delta vs Omicron-BA.1 competition
333 experiment (8 % mortality). A comparable high mortality rate was also seen in association
334 with Alpha in our earlier study of paired VOC competitions including Alpha, Beta, and
335 SARS-CoV-2^{D614G} (Ref¹⁰), suggesting that the degree of pathogenicity in the Syrian hamster
336 correlates with the respective replicative fitness in this model.

337 Another surprising finding in our study was that Omicron-BA.1 does not productively
338 replicate in ferrets. While we see, in agreement with the epidemiological situation in humans,
339 that the Delta variant vastly predominates over the Alpha variant in terms of early replication
340 and especially transmission in the ferret model, we observed that Omicron-BA.1 infection is
341 abortive. The remarkable observations of Omicron-BA.1 being outcompeted by the Delta
342 variant in naïve Syrian hamsters and the complete block of ferret susceptibility towards
343 Omicron-BA.1 provides further evidence to an adaptation of this variant towards humans.
344 This also makes it rather unlikely that the Omicron variant evolved in an animal reservoir.

345 It was therefore important to include animal models that are based on the usage of the
346 authentic hACE2 receptor. The hACE2 knock-in mice have previously shown to be a valuable
347 model for SARS-CoV-2 replication in the URT as they show robust SARS-CoV-2 replication
348 with only mild or sub-clinical disease. The observation that also in this model Delta
349 outcompeted Omicron-BA.1 and similarly, the corresponding Delta spike clone SARS-CoV-
350 2^{S-Delta} outcompeted the Omicron-BA.1 spike clone SARS-CoV-2^{S-Omicron}, suggests that the
351 intrinsic replicative fitness of Delta is still higher than that of Omicron-BA.1 once a
352 productive replication is established within the infected host and that this phenotype is
353 mediated by the spike genes of Delta and Omicron-BA.1. Notably, the infection of hACE2-KI
354 mice with the Delta isolate resulted for the first time in our hands in evident lung pathology
355 and body weight loss, suggesting that this model recapitulates the increased pathogenicity of
356 Delta in humans and that it will receive further attention in future studies that aim at assessing
357 SARS-CoV-2 variants with high pathogenicity.

358 Notably, by using hNEC and hBEC cultures we were able to detect an accelerated growth of
359 Omicron-BA.1 in hNECs within the first 48 hours post infection that reflects the observed
360 shorter incubation period of Omicron-BA.1 versus previous SARS-CoV-2 variants in humans.
361 In contrast, in hBECs, Omicron-BA.1 replication is limited to lower peak titers, suggesting
362 reduced replication in bronchial and lung tissue as previously demonstrated in lung explant *ex*
363 *vivo* tissue cultures¹⁶. Importantly, this phenotype is also seen by infections with the Omicron-
364 BA.1 spike clone SARS-CoV-2^{S-Omicron}, demonstrating that it is spike-mediated. Moreover,
365 the reduced replication of SARS-CoV-2^{S-Omicron} in the lungs of K18-hACE2 mice and the
366 resulting mild pathology confirms that this phenotype is indeed spike-mediated and likely
367 contributes to the reduced pathogenicity of Omicron-BA.1 as seen in humans. Of note, the
368 increased replication, pathology, and clinical scores of SARS-CoV-2^{S-Delta} point to the

369 opposite phenotype of increased pathogenicity that is according to our study also mediated by
370 the spike gene.

371 Finally, our study illustrates the degree of immune evasion of Omicron-BA.1 in comparison
372 to Delta and the index virus SARS-CoV-2^{D614G}. The mRNA vaccine is well matched to the
373 index virus SARS-CoV-2^{D614G}, and accordingly, vaccinated mice are well protected.
374 Recently, it has been shown that the replicative and transmissive fitness advantage of
375 Omicron against Delta changes in favor of Omicron when hamsters are vaccinated,
376 highlighting the influence of Omicron-associated immune escape potential and the importance
377 of the immune status on virus selection ¹⁷. Our data from vaccinated mice extend this finding
378 by using an animal model with the authentic hACE2 receptor, and by assigning this context-
379 specific phenotypic change to the Omicron-BA.1 spike gene.

380 In summary, we provide here a comprehensive and comparative analysis of the Omicron-
381 BA.1 phenotype by using several advanced *in vitro* and *in vivo* systems and different VOCs.
382 We demonstrate that Omicron-BA.1 displays a remarkable evolutionary and phenotypic jump
383 that impacts virus replication, host and tissue tropism, pathogenicity, and immune escape,
384 with the spike gene being a key determinant of these phenotypic changes.

385

386 Acknowledgements

387 For animal care, we thank Frank Klipp, Doreen Fiedler, Christian Lipinski, Harald Manthei
388 and Steffen Kiepert (Friedrich-Loeffler-Institut); I. Wymann, R. Troxler, K. Sliz, and D.
389 Brechbühl (Institute of Virology and Immunology). For technical assistance, we thank
390 Mareen Lange, Christian Korthase, Patrick Zitzow, Silvia Schuparis, and Bianka Hillmann
391 (Friedrich-Loeffler-Institut). We thank Matthias Lenk for preparing and providing cell
392 cultures and media; and Jacqueline King, Anne Pohlmann, and Lina Stacker for sequencing
393 assistance (Friedrich-Loeffler-Institut). We thank Dr. H.Y. Stoller-Kwan and Dr F. Gregorini,

394 Inselspital, University Hospital Bern, for reagents. We thank Artur Summerfield (Institute of
395 Virology and Immunology) for internal financial support. We thank Georg Kochs from the
396 University of Freiburg, Germany for the SARS-CoV-2 isolate. We thank Franziska. Suter-
397 Riniker and Pascal. Bittel, Institute for Infectious Diseases, University of Bern, for providing
398 clinical samples. VeroE6/TMPRSS2 cells were provided by the NIBSC Research Repository,
399 UK with thanks to Dr Makoto Takeda. This work was supported by the Swiss National
400 Science Foundation (SNSF) grants no. 31CA30_196062 (CB, RD), 31CA30_196644 (VT,
401 RD), 310030_173085 (VT), 310030_179260 (RD); the European Commission, Marie
402 Skłodowska-Curie Innovative Training Network ‘HONOURS’, grant agreement no. 721367
403 (VT, RD); Core funds of the University of Bern (VT, RD); Core funds of the German Federal
404 Ministry of Food and Agriculture (MB); the Deutsche Forschungsgemeinschaft (DFG),
405 Project no. 453012513 (MB); the Horizon 2020 project “VEO”, grant agreement no. 874735
406 (MB), the Lungenliga Bern, Switzerland (MPA). The funders had no role in study design,
407 data collection and analysis, decision to publish, or preparation of the manuscript. The authors
408 would like to thank all study participants and their families.

409

410 **Author contributions**

411 TB, NJH, AT, JNK, JS, NE, LU, RD, DH, MPA, CB, MBe, VT conceived the study ; TB,
412 NJH, AT, JS, NE, LU, CD, SS, BST, IBV, DH performed most of the experiments ; BH,
413 NGFL, EAM, AB, CW, DH, KW, AG, LT, VF, HS, MBr, BIOE, BZ, GB, AK, KS, SO,
414 RML, MW, CM, PD, TMM, MFC, AR, MW, SC did experimental work and/or provided
415 essential experimental systems and reagents ; JNK, CW performed sequencing including
416 computational analyses; TB, NJH, AT, JNK, JS, NE, LU, DH, MPA, CB, MBe, VT wrote the
417 manuscript and made the figures. All authors read and approved the final manuscript.

418

419 **Competing interests**

420 Authors declare that they have no competing interests.

421 **Data and materials availability**

422 All data are available in the main text or the supplementary materials.

423

424 **References**

425 1 Motozono, C. *et al.* SARS-CoV-2 spike L452R variant evades cellular immunity and
426 increases infectivity. *Cell Host Microbe* **29**, 1124-1136 e1111, doi:S1931-
427 3128(21)00284-5 [pii]
428 10.1016/j.chom.2021.06.006 (2021).

429 2 Liu, Y. *et al.* Delta spike P681R mutation enhances SARS-CoV-2 fitness over Alpha
430 variant. *bioRxiv*, 2021.2008.2012.456173, doi:10.1101/2021.08.12.456173 (2021).

431 3 ECDC. Implications of the emergence and spread of the SARSCoV-2 B.1.1. 529
432 variant of concern (Omicron), for the EU/EEA. (2021).

433 4 Cele, S. *et al.* Omicron extensively but incompletely escapes Pfizer BNT162b2
434 neutralization. *Nature* **602**, 654-656, doi:10.1038/s41586-021-04387-1 (2022).

435 5 Wilhelm, A. *et al.* Reduced Neutralization of SARS-CoV-2 Omicron Variant by
436 Vaccine Sera and Monoclonal Antibodies. *medRxiv*, 2021.2012.2007.21267432,
437 doi:10.1101/2021.12.07.21267432 (2021).

438 6 CoVariants. *Overview of Variants in Countries*, <<https://covariants.org/per-country>>
439 (2022).

440 7 Gu, H. *et al.* Recombinant BA.1/BA.2 SARS-CoV-2 Virus in Arriving Travelers,
441 Hong Kong, February 2022. *Emerg Infect Dis* **28**, doi:10.3201/eid2806.220523
442 (2022).

443 8 de Vries, R. D. *et al.* Animal models of SARS-CoV-2 transmission. *Current Opinion
444 in Virology* **50**, 8-16, doi:<https://doi.org/10.1016/j.coviro.2021.06.007> (2021).

445 9 Zhou, B. *et al.* SARS-CoV-2 spike D614G change enhances replication and
446 transmission. *Nature* **592**, 122-127, doi:10.1038/s41586-021-03361-1

447 10.1038/s41586-021-03361-1 [pii] (2021).

448 10 Ulrich, L. *et al.* Enhanced fitness of SARS-CoV-2 variant of concern Alpha but not
449 Beta. *Nature* **602**, 307-313, doi:10.1038/s41586-021-04342-0

450 10.1038/s41586-021-04342-0 [pii] (2022).

451 11 Plante, J. A. *et al.* Spike mutation D614G alters SARS-CoV-2 fitness. *Nature* **592**,
452 116-121, doi:10.1038/s41586-020-2895-3 (2021).

453 12 Touret, F. *et al.* Replicative Fitness of a SARS-CoV-2 20I/501Y.V1 Variant from
454 Lineage B.1.1.7 in Human Reconstituted Bronchial Epithelium. *mBio* **12**, e0085021,
455 doi:10.1128/mBio.00850-21 (2021).

456 13 Port, J. R. *et al.* Increased small particle aerosol transmission of B.1.1.7 compared
457 with SARS-CoV-2 lineage A in vivo. *Nature Microbiology* **7**, 213-223,
458 doi:10.1038/s41564-021-01047-y (2022).

459 14 McMahan, K. *et al.* Reduced Pathogenicity of the SARS-CoV-2 Omicron Variant in
460 Hamsters. *bioRxiv*, 2022.2001.2002.474743, doi:10.1101/2022.01.02.474743 (2022).

461 15 Abdehnabi, R. *et al.* The omicron (B.1.1.529) SARS-CoV-2 variant of concern does
462 not readily infect Syrian hamsters. *bioRxiv*, 2021.2012.2024.474086,
463 doi:10.1101/2021.12.24.474086 (2021).

464 16 Hui, K. P. Y. *et al.* SARS-CoV-2 Omicron variant replication in human bronchus and
465 lung ex vivo. *Nature* **603**, 715-720, doi:10.1038/s41586-022-04479-6 (2022).

466 17 Yuan, S. *et al.* The SARS-CoV-2 Omicron (B.1.1.529) variant exhibits altered
467 pathogenicity, transmissibility, and fitness in the golden Syrian hamster model.
468 *bioRxiv*, 2022.2001.2012.476031, doi:10.1101/2022.01.12.476031 (2022).

469

470 **Figure legends**

471 **Fig. 1: Enhanced replication of Omicron-BA.1 in nasal but not bronchial epithelial cell**
472 **cultures. a)** Lineage-defining mutations (LDM) present in VOCs Delta, Omicron-BA.1,
473 SARS-CoV-2^{S-Delta} and SARS-CoV-2^{S-Omicron}, and Omicron-BA.1 subdomain clones (RBD,
474 NTD, CS) are depicted. Genome sequences were compared to the SARS-CoV-2^{D614G} WT
475 virus and only LDM classified as missense mutations, deletions, or insertions are illustrated.
476 The D614G mutation, which is present in all viruses, is highlighted in red, while the
477 mutations highlighted in orange are either present in both Delta and Omicron (NSP12:P314L)
478 or in Omicron, S-Omicron, RBD-Omicron, Delta, and S-Delta (T478K), but not in SARS-
479 CoV-2^{D614G}. **b)** The plaque sizes caused by the respective viruses in 6-well plates after 2 dpi
480 are shown. Plaque sizes were measured in Adobe Illustrator. Statistical significance was
481 determined using ordinary one-way Anova and p-values were adjusted using Tukey's
482 multiple-comparison test; *P<0.05, **P<0.01, ***P<0.001, ****P<0.0001. Results from
483 statistical testing where each virus was compared to SARS-CoV-2^{D614G} WT virus are
484 demarcated with the red asterisks, whereas the black asterisks show the results from the
485 comparison of the Omicron spike subdomain clones to Omicron. **c-d)** Human nasal (NEC)
486 and bronchial epithelial cell (BEC) cultures were infected with 10⁴ TCID₅₀ of the SARS-CoV-
487 2 variants from the apical side and incubated at 33°C (NECs) or 37°C (BECs) for 1 hour.
488 Virus titers were assessed by standard TCID₅₀ assays on Vero TMPRSS2 cells. Statistical
489 significance was determined using two-way ANOVA and P values were adjusted using
490 Tukey's multiple-comparison test; *P<0.05, **P<0.01, ***P<0.001, ****P<0.0001. **e-g)**
491 NECs, BECs, or lung explants were infected with virus mixtures at a 1:1 ratio based on
492 genome equivalents (GE) calculated by qPCR. Apical washes were collected at 2 and 6 days
493 post infection (dpi) for the NECs and BECs and 2 dpi for lung explants. RNA was extracted
494 from apical washes and sequenced on the MinION platform (Oxford Nanopore

495 Technologies). Virus ratios were calculated for each donor based on the mean frequency of
496 unique LDM mutations for each virus present in the mixture (for more details see Extended
497 Data Fig. 1). Values shown represent the mean ratio per donor (circles) and the mean ratio per
498 time point (bars) for each virus mixture. Each data point represents one biological replicate.

499

500 **Fig. 2: *In vivo* competitive co-infection and single infection studies with VOC Delta and**
501 **Omicron-BA.1 in Syrian hamsters and ferrets.** Simultaneous co-inoculation of six donor
502 hamsters and ferrets each with a Delta:Omicron-BA.1 mixture (hamster, ratio of 1:2.16, total
503 $10^{4.5}$ TCID₅₀/hamster and ferrets, ratio of 1:1.43, total $10^{4.75}$ TCID₅₀/ferret) and sequential
504 pairwise co-housing of contact animals. All data were quantified using RT-qPCR. Pie chart
505 size represents the total amount of viral RNA (vRNA) detected in each sample (exact vRNA
506 equivalents are found in Source Data files and the coloring shows the individual VOC ratio.
507 Animal silhouettes are colored according to the dominant (>66%) VOC. Limit of detection
508 was set at 10^3 vRNA copies per mL. **a)** Nasal washings of Donor and Contact I+II Syrian
509 hamster pairs from 1 to 21 dpi. **b)** vRNA in URT and LRT of donor hamsters at 4 dpi. **c)**
510 Nasal washings of Delta and Omicron-BA.1 co-inoculated Donor and respective Contact
511 ferrets for the 21-day infection period. **d-e)** Antibody detection in hamsters (d) and ferrets (e)
512 via VNT₁₀₀ and RBD-ELISA after simultaneous Delta and Omicron-BA.1 co-inoculation
513 shown for donor (D), contact (C), contact I (CI), and contact II (CII) animals. Specific
514 neutralizing capacity of sera against the Delta (pink) and Omicron-BA.1 (yellow) virus pair
515 were analyzed. Reactivity of sera below 1:32 pre-dilution was considered negative.
516 Generalized seroreaction was also determined by RBD-ELISA (black dots). **f)** vRNA
517 detection and seroreactivity in ferrets after infection with single virus (Delta or Omicron-
518 BA.1); donor animals (solid line) and contact animals (dashed line). Limit of detection was

519 set at 10^3 vRNA copies per mL and for antibody detection at >0.2 (questionable) and >0.3
520 (positive).

521

522 **Fig. 3: Delta spike mutations drive enhanced fitness in humanized mice. a-e)** hACE2-KI
523 mice (7 to 16 week-old male) were intranasally inoculated with $10^{4.3}$ tissue culture infectious
524 dose 50 (TCID₅₀) of Delta or Omicron isolates. **a)** relative body weight loss after infection. **b)**
525 Viral copies per mL of oropharyngeal swabs or per lung and nose sample quantified using E-
526 gene probe-specific RT-qPCR. **c)** Infectious virus titers from the lung and nose samples
527 determined using TCID₅₀ assays in VeroE6-TMPRSS2 cells. **d-e)** Histopathological score and
528 hematoxylin and eosin staining from Delta and Omicron infected lung sections at 2 and 4 dpi.
529 Perivasular and peribronchiolar lymphohistiocytic inflammation are highlighted with an
530 arrow, and the higher magnification represented in the lower panel corresponds to the areas
531 highlighted by a square in the upper panel. Scale bars, 500 (upper panel) and 100 μ m (lower
532 panel). Data are mean \pm s.d. from the indicated number of biological replicates from a single
533 experiment. The color key in a also applies to b, c and d. Statistical significance was
534 determined using an unpaired Student t-test; *P < 0.05, **P < 0.01, ***P < 0.001,
535 ****P < 0.0001. **f-g)** hACE2-KI mice (7 to 19 week-old female, n=6/group) were intranasally
536 inoculated with 10^4 TCID₅₀ of a 1:1 mix of **f)** Delta and Omicron, or **g)** SARS-CoV-2^{S-Delta}
537 and SARS-CoV-2^{S-Omicron}. qPCR quantification of the ratio of the two variants or recombinant
538 viruses present in the inoculum is reported. Oropharyngeal swabs were collected 1 and 2 dpi;
539 lung, nose tissues were collected on 2 dpi. Pie charts show the ratio of variants detected in
540 each sample at the indicated dpi. Pie chart sizes are proportional to the total number of viral
541 genome copies per ml (swabs) or per sample (tissues), as shown in the legend on the right.
542 Grey pies indicate values below the LOD (i.e., 10^3 viral RNA copies per mL/sample). Mouse
543 silhouettes are colored to indicate the dominant SARS-CoV-2 variant (>66%) in the last

544 positive swab sample from the corresponding mouse. KI numbers 1 to 12 denote individual
545 hACE2-KI mice. Data was obtained from one experiment.

546

547 **Fig. 4: mRNA vaccine induced reduction in replication and pathogenesis of SARS-CoV-
548 2 clones in K18-hACE2 transgenic mice. a)** Female K18-hACE2 transgenic mice (7 to 15
549 weeks old) were immunized intramuscularly with a single dose of 1 μ g of mRNA-Vaccine
550 Spikevax (Moderna). After two weeks the neutralizing antibody titers against SARS-CoV-2
551 were determined (Extended Data Fig. 10). Later, mice were intranasally inoculated with 10^4
552 tissue culture infectious dose 50 (TCID₅₀) of SARS-CoV-2^{614G}, SARS-CoV-2^{S-Delta}, or SARS-
553 CoV-2^{S-Omicron}. **b)** The change in body weight and clinical scores (Extended Data Fig. 10) of
554 the mice were monitored daily. Only the unvaccinated mice infected with SARS-CoV-2^{614G}
555 and SARS-CoV-2^{S-Delta} showed noticeable weight loss. **c)** Oropharyngeal swabs, lung and nose
556 samples of the infected mice were collected at 2 or 6 days post-infection (dpi) to determine
557 the viral load (n=4 for each virus). Viral RNA-dependent RNA polymerase (RdRp) gene
558 copies were quantified using probe-specific RT-qPCR. **d)** Infectious virus titers from the lung
559 and nose samples were determined using TCID₅₀ assays in VeroE6-TMPRSS2 cells. **e)**
560 Hematoxylin and eosin stain (left panel) and immunohistochemical analysis specific for
561 SARS-CoV-2 nucleocapsid protein (right panel) of lung sections in vaccinated (A) and
562 unvaccinated mice (B) at 2 and 6 dpi following infection with SARS-CoV-2^{614G} (n=3), SARS-
563 CoV-2^{S-Delta} (n=3), and SARS-CoV-2^{S-Omicron} (n=4). Consolidated lung areas are highlighted
564 with a star, and perivascular and peribronchiolar lymphohistiocytic inflammation highlighted
565 with an arrow. Scale bars, 500 μ m. Data are mean \pm s.d. from the indicated number of
566 biological replicates. The color key in b also applies to c and d. Statistical significance was
567 determined using two-way ANOVA (a-d) and P values were adjusted using Tukey's

568 multiple-comparison test; *P < 0.05, **P < 0.01, ***P < 0.001, ****P < 0.0001. Data were
569 obtained from one experiment. Each data point represents one biological replicate.

570

571 **List of Extended Data and Supplementary Information files**

572 Extended Data Figures 1 to 10

573 Extended Data Table 1

574 Supplementary Information Tables 1-4

575

576

577 **Methods**

578

579 **Cells and culture conditions**

580 At IVI, IBSCVeroE6 (Vero C1008, ATCC) and VeroE6/TMPRSS2 cells (NIBSC) were cultured
581 in Dulbecco's modified Eagle's medium (DMEM). BHK-SARS-N (BHK-21 cells expressing
582 the N protein of SARS)¹⁸ were grown in minimal essential medium (MEM). Both media were
583 supplemented with 10% (v/v) fetal bovine serum, 1% (w/v) non-essential amino acids, 100
584 IU/mL penicillin, 100 µg/mL streptomycin µg/ml and the cell lines maintained at 37 °C in a
585 5% CO₂ atmosphere.

586 Vero E6 cells at FLI (Collection of Cell Lines in Veterinary Medicine CCLV-RIE 0929) were
587 cultured using a mixture of equal volumes of Eagle MEM (Hanks' balanced salts solution)
588 and Eagle MEM (Earle's balanced salts solution) supplemented with 2 mM L-Glutamine,
589 nonessential amino acids adjusted to 850 mg/L, NaHCO₃, 120 mg/L sodium pyruvate, 10%
590 fetal bovine serum (FBS), pH 7.2.

591 Calu-3 cells (HTB-55, American Type Culture Collection (ATCC), Manassas, VA, USA)
592 were propagated in Dulbecco's modified Eagle Medium–GlutaMAX, supplemented with 10%
593 (v/v) heat-inactivated fetal bovine serum, 100 mg/mL streptomycin, 100 IU/mL penicillin, 1%
594 (w/v) non-essential amino acids, and 15 mM 4-(2-hydroxyethyl)-1-piperazineethanesulfonic
595 acid (HEPES, Gibco, Gaithersburg, MD, USA). Cells were maintained at 37 °C in a
596 humidified incubator with 5% CO₂.

597

598 **Viruses**

599 Viruses are listed in Extended Data Table 1. Viruses were cultivated on VeroE6, Vero-
600 TMPRSS2, or Calu-3 cells and sequence verified by performing whole-genome NGS

601 sequencing (see below). For the hamster and ferret infection studies SARS-CoV-2 Alpha
602 (hCoV-19/Germany/NW-RKI-I-0026/2020, L4549, SARS-CoV-2 B.1.1.7 NW-RKI-I-
603 0026/2020 passage 3 of EPI_ISL_751799), one silent mutation in the ORF1a (sequence
604 position 11741), SARS-CoV-2 Delta AY.127 (hCoV-19/Switzerland/BE-IFIK-918-
605 4879/2021, L5109, passage of EPI_ISL_1760647) and SARS-CoV-2 Omicron-BA.1 (BA.1
606 (hCoV-19/Germany/HE-FFM-30318738/2021, passage of EPI_ISL_6959868) was used. The
607 Omicron-BA.1 isolate was from the Institute of Medical Virology, University Hospital
608 Frankfurt, Goethe University, Frankfurt am Main, Germany. For the hamster and ferret
609 competition experiments, respective Alpha, Delta or Omicron-BA.1 viruses were propagated
610 (three passages for Alpha, two passages for Omicron-BA.1, one passage for Delta) on Vero
611 E6 cells (Collection of Cell Lines in Veterinary Medicine CCLV-RIE 0929) using a mixture
612 of equal volumes of Eagle MEM (Hanks' balanced salts solution) and Eagle MEM (Earle's
613 balanced salts solution) supplemented with 2 mM L-Glutamine, nonessential amino acids
614 adjusted to 850 mg/L, NaHCO₃, 120 mg/L sodium pyruvate, 10% fetal bovine serum (FBS),
615 pH 7.2. The virus was harvested after 72h, titrated on Vero E6 cells and stored at -80°C until
616 further use.

617 For *in vitro* experiments, Delta and Omicron-BA.1 were isolated at the University of Bern.
618 Briefly, an aliquot of 250 µl of SARS-CoV-2 positive patient material (Delta;
619 EPI_ISL_1760647, Omicron-BA.1; EPI_ISL_7062525) was centrifuged for 5 minutes at
620 room temperature at 1× relative centrifugal force (RCF). 200 µl of clinical material was
621 transferred to confluent Calu-3 cells and incubated for 2-3 days at 37°C in a humidified CO₂-
622 incubator (5%). Virus containing supernatant was cleared from cell debris through
623 centrifugation for 5 min at 500×RCF before aliquoting and storage at -80 °C. All virus stocks
624 were sequenced with Nanopore sequencing technology using a revised ARTIC midnight
625 protocol (Fragment 28 update) allowing sequencing of both Delta and Omicron-BA.1

626 variants. SARS-CoV-2 Delta. Sequence verified stocks at passage 3 were used. For the
627 experiments in hACE2-KI mice, the Delta isolate (EPI_ISL_2535433)¹⁹ was kindly provided
628 by Georg Kochs, Institute of Virology, Freiburg, Germany and Omicron-BA.1 was isolated at
629 the University of Bern (EPI_ISL_7062525). The TCID₅₀ titers have been determined on
630 VeroE6 and were calculated according to the Spearman-Kaerber formula.

631

632 **Generation of infectious cDNA clones using transformation-associated recombination
633 cloning and rescue of recombinant viruses**

634 We used the in-yeast transformation-associated recombination (TAR) cloning method as
635 described previously with few adaptations to generate SARS-CoV-2^{S-Delta} and SARS-CoV-2^{S-}
636 Omicron²⁰. In sum, the whole SARS-CoV-2 genome was encoded in 12 overlapping DNA
637 fragments. These so-called WU-Fragments and a TAR-vector are homologous recombined in
638 yeast forming the yeast artificial chromosome (YAC). WU-Fragments 9 and 10 covering the
639 spike region were replaced by newly generated and overlapping PCR products. To introduce
640 the variant specific mutations into the spike gene, we used 50 bp primers containing the
641 desired nucleotide changes in combination with YAC DNA templates from previously cloned
642 viruses (Supplementary Information Table 3). Also, by using these 50 bp long primers
643 homologous overlaps between the PCR products were created. Six PCR reactions using the
644 Q5® High-Fidelity DNA Polymerase (NEB) were performed to replace WU-Fragment 9 and
645 10 to create the SARS-CoV-2^{S-Delta}. To create the SARS-CoV-2^{S-Omicron} and its sub spike
646 clones overlapping PCR products via RT from Omicron RNA template were done. In brief,
647 cDNA was generated from RNA (Omicron-BA.1; EPI_ISL_7062525) by LunaScript RT
648 SuperMix (NEB). PCR reactions using Q5® High-Fidelity DNA Polymerase were performed
649 with the primers and templates described in Supplementary Information Table 3. The
650 resulting PCR products were mixed and matched for Omicron-Spike, -NTD, -RBD and -CS to

651 replace WU-Fragment 9 and 10. All PCR products were purified by the High Pure PCR
652 Product Purification Kit (Roche) before being used for TAR cloning.

653 In vitro transcription was performed for EagI-cleaved YACs and PCR-amplified SARS-CoV-
654 2 N gene using the T7 RiboMAX Large Scale RNA production system (Promega) as
655 described previously²⁰. Transcribed capped mRNA was electroporated into baby hamster
656 kidney (BHK-21) cells expressing SARS-CoV N protein. Electroporated cells were co-
657 cultured with susceptible Vero E6TMPRSS cells to produce passage 0 (P.0) of the
658 recombinant viruses. Subsequently, progeny viruses were used to infect fresh TMPRRS cells
659 to generate P.1 stocks for downstream experiments.

660 To introduce the variant specific mutations into the spike gene to create the SARS-CoV-2^S-
661 ^{Delta}, we used 50 bp primers containing the desired nucleotide changes in combination with
662 YAC DNA templates from previously cloned mutations (Supplementary Information Table
663 3). Also, by using these primers, 50 bp homologous overlap between the PCR products were
664 created. Six PCR reactions using the Q5® High-Fidelity DNA Polymerase (NEB) were
665 performed.

666 To create the SARS-CoV-2^{S-Omicron} and its sub spike clones overlapping PCR products via RT
667 from Omicron RNA template were done. In brief, cDNA was generated from RNA (isolated
668 of supernatant of Omicron isolate of RD infected cells) by LunaScript RT SuperMix (NEB).
669 PCR reactions with Q5® High-Fidelity DNA Polymerase (NEB) were performed with the
670 primers and templates described in Supplementary Information Table 3. These primers were
671 chosen to produce overlapping PCR fragments, thus contain the omicron specific mutations.
672 All PCR products were purified by the High Pure PCR Product Purification Kit (Roche)
673 before TAR cloning.

674 These purified PCR products were used to replace WU-Fragments 9 and 10 (covering the
675 spike region) in our set of WU-Fragments. These WU-Fragments encoding the whole SARS-

676 CoV2 genome were previously described²⁰. The WU-Fg 1.3-8, 11,12 and the newly created
677 PCR fragments containing the variant specific mutations and with 50 bp homologous
678 overlaps, were then used for the in-yeast TAR cloning method as described previously²⁰ to
679 generate infectious cDNA clones.

680

681 **Virus replication kinetics on human primary airway cells**

682 hNEC and hBEC cultures were infected with 10^4 TCID₅₀ of the SARS-CoV-2 variants listed
683 in the Extended Data Table 1. Viruses were diluted in HBSS (Gibco), inoculated on the apical
684 side, and incubated for 1 hour at 33°C in case of hNECs or 37°C in case of hBECs.
685 Subsequently, the inoculum was removed, and the cells were washed three times with 100 µl
686 of HBSS. The third wash was collected as the 1 hpi time point. For the duration of the
687 experiment, hNECs and hBECs were incubated in a humidified incubator with 5% CO₂ at
688 33°C or 37°C, respectively. To measure virus progeny release, apical washes were performed
689 every 24 hours up to 96 hpi. 100 µl HBSS were incubated on the apical side for 10 min prior
690 to the respective time point and subsequently collected, diluted 1:1 with virus transport
691 medium (VTM), and stored at -80°C for later analysis.

692 Virus titers were assessed by standard TCID₅₀ assays on Vero-TMPRSS2 cells. In short,
693 2x10⁴ cells/well were seeded in a 96-well plate one day before the titration and were then
694 inoculated with a 10-fold serial dilution of the prior collected apical washes. Four technical
695 replicates were performed for each sample. Cells were then incubated for 72 hours at 37°C in
696 a humidified incubator with 5% CO₂. Subsequently, cells were fixed with 4% (v/v) buffered
697 formalin (formafix) and stained with crystal violet. Infected wells were counted, and TCID₅₀
698 was calculated according to the Spearman-Kaerber formula.

699

700 **Competition assay in hNEC and hBEC cultures**

701 Inoculum mixtures were generated by mixing the respective viruses at a 1:1 ratio based on
702 genome equivalents (GE) determined by qPCR including RNA standard. Each mixture
703 contained 6×10^7 GE of each respective virus. hNECs and hBECs were infected with inoculum
704 mixtures apically and incubated for 1 hour at 33°C or 37°C respectively. Afterwards, inocula
705 were removed and the cells were washed three times with 100 µl HBSS (Gibco). For the
706 duration of the experiment, the hNECs and hBECs were incubated in a humidified incubator
707 with 5% CO₂ at 33°C or 37°C, respectively. Apical washes were performed and collected at 2,
708 4 and 6 dpi. 100 µl HBSS were incubated on the apical side for 10 min prior to the respective
709 time point and subsequently collected, mixed with 300 µl DNA/RNA Shield lysis buffer
710 (Zymo Research) and stored at -80°C for later analysis.

711

712 **Nanopore sequencing workflow**

713 Virus stocks, inoculum mixtures, and samples from competition assays in NECs, BECs, and
714 lung explants were sequenced using the MinION sequencer (Oxford Nanopore Technologies)
715 following the ARTIC nCoV-2019 sequencing protocol V3 (LoCost)
716 (<https://protocols.io/view/ncov-2019-sequencing-protocol-v3-locost-bh42j8ye>) with the
717 following modifications: the Midnight primer scheme (1200 bp amplicons) was used to
718 perform the multiplex PCR (<https://www.protocols.io/view/sars-cov2-genome-sequencing-protocol-1200bp-amplic-rm7vz8q64vx1/v6>) instead of the ARTIC V3 primer scheme. In
719 addition, two extra Omicron-specific primers (SARSCoV_1200_Omicron_24_L: 5'- GCT
720 GAA TAT GTC AAC AAC TCA TAT GA -3' and SARSCoV_1200_Omicron_28_L: 5'-
721 TTT GTG CTT TTT AGC CTT TCT GTT -3') were added to Pool 2 of the multiplex PCR to
722 achieve similar levels of amplification for all viruses sequenced.

724 RNA was extracted for all samples using either the Quick-RNA Viral Kit (Zymo Research) or
725 the NucleoMag VET kit (Machery-Nagel) according to the manufacturer's guidelines on a
726 Kingfisher Flex Purification system (Thermofisher). Extracted RNA was assessed using the
727 TaqPath COVID-19 CE-IVD RT-PCR Kit (Thermofisher) and cDNA was prepared using the
728 LunaScript RT SuperMix Kit (Bioconcept). Subsequently, a multiplex PCR was used to
729 generate overlapping 1200 bp amplicons that span the length of the SARS-CoV-2 genome for
730 all used virus VOCs. The Q5 Hot Start High-Fidelity 2X Master Mix (Bioconcept) was used
731 for the multiplex PCR reaction. For library preparation, all samples were barcoded using the
732 Native Barcoding Kit 96 (Oxford Nanopore Technologies, SQK-NBD112-96). Libraries were
733 then loaded onto a R9.4.1 flow cell on a MinION sequencer (Oxford Nanopore Technologies)
734 and monitored using the MinKNOW software (Version 21.11.9). A no-template negative
735 control from the PCR amplification step was prepared in parallel and sequenced on each flow
736 cell.

737 Live GPU basecalling was performed using Guppy v.5.1.15 (Oxford Nanopore technologies)
738 in high-accuracy mode. Following sequencing, downstream analysis was performed using a
739 modified version of the nCoV-2019 novel coronavirus bioinformatics protocol (ARTIC
740 Network, <https://artic.network/ncov-2019/ncov2019-bioinformatics-sop.html>). The command
741 'artic gupplex' was used to filter "pass" reads based on length with --max-length set to 1400.
742 The 'artic minion' command was then used to align the filtered reads to the Wuhan-Hu-1
743 reference genome (accession MN908947.3) with the 'normalise' parameter set to 500. BAM
744 alignment files generated using the ARTIC pipeline were subsequently used as input to call
745 variants in longshot (v.0.4.4). An input VCF file containing VOC Delta and Omicron BA.1
746 mutations was provided to longshot in order to genotype specific nucleotide sites. Output
747 VCF files for each sample were used as input for downstream analysis in R v.4.1.3.

748 Calculations were performed on UBELIX (<http://www.id.unibe.ch/hpc>), the HPC cluster at
749 the University of Bern.

750 Downstream analysis of VCF files for each sample was performed using a custom script in R
751 v.4.1.3. Briefly, each VCF file was first filtered to exclude mutations shared between both
752 viruses in the mixture, non-lineage-defining mutations, sites that were difficult to call (e.g.,
753 sites with unique but overlapping mutations or with a high number of ambiguous calls), and
754 mutations called with a depth of coverage lower than 100. Sequencing depth across the entire
755 genome was also checked each sample along with the frequency of any ‘shared’ mutations in
756 each virus mixture (in these cases the frequency should be close to 1). Following filtering and
757 quality control checks, the remaining variant calls were used to calculate the mean mutation
758 frequencies for each virus on a per sample basis (Extended Data Figure 1). Finally, the mean
759 \pm sd virus ratio was calculated for each virus mixture at each time point for NEC, BEC, and
760 lung explants.

761

762 **Ion Torrent Sequencing**

763 Virus stocks was sequenced using a generic metagenomics sequencing workflow as described
764 previously (Wylezich et al. 2018) with some modifications. For reverse-transcribing RNA
765 into cDNA, SuperScriptIV First-Strand cDNA Synthesis System (Invitrogen, Germany) and
766 the NEBNext Ultra II Non-Directional RNA Second Strand Synthesis Module (New England
767 Biolabs, Germany) were used, and library quantification was done with the QIAseq Library
768 Quant Assay Kit (Qiagen, Germany). Libraries were sequenced using an Ion 530 chip and
769 chemistry for 400 base pair reads on an Ion Torrent S5XL instrument (Thermo Fisher
770 Scientific, Germany).

771

772 **Ethics statements for human subjects and animal experimentation**

773 All ferret and hamster experiments were evaluated by the responsible ethics committee of the
774 State Office of Agriculture, Food Safety, and Fishery in Mecklenburg–Western Pomerania
775 (LALLF M-V) and gained governmental approval under registration number LVL MV
776 TSD/7221.3-1-004/21.

777 Mouse studies were approved by the Commission for Animal Experimentation of the
778 Cantonal Veterinary Office of Bern and conducted in compliance with the Swiss Animal
779 Welfare legislation and under license BE43/20.

780 Lung tissue for the generation of human precision-cut lung slices (PCLSs) and human
781 bronchial epithelial cells (hBECs) was obtained from patients undergoing pulmonary
782 resection at the University Hospital of Bern, Inselspital, Switzerland, and the Cantonal
783 Hospital of St. Gallen, Switzerland, respectively. Written informed consent was obtained for
784 all the patients and the study protocols were approved by the respective local Ethics
785 Commissions (KEK-BE_2018-01801, EKSG 11/044, and EKSG 11/103).

786

787 **Hamster competition studies**

788 The study outline for the hamster competition studies can be seen in Extended Data Figure 2a.
789 Six Syrian hamsters (*Mesocricetus auratus*) (Janvier Labs) were inoculated intranasally under
790 a brief inhalation anesthesia with a 70 μ l mixture of two respective SARS-CoV-2 VOC (Alpha
791 versus Delta and Delta versus Omicron-BA.1), referred to as donor hamsters. Each inoculum,
792 as well as the single viruses were backtitrated followed by determination of VOC ratio by
793 dividing the TCID₅₀/mL values of single VOC1 by VOC2. One day following inoculation of
794 the donor hamsters, we co-housed six naïve contact hamsters (Contact I) in a 1:1 setup. The

795 donor hamsters were removed from the experiment on 4 dpi for organ sampling (RT-qPCR)
796 and have been replaced by another naïve contact hamster (Contact II).

797 Viral shedding was monitored by nasal washings in addition to a daily physical examination
798 and body weighing routine. Nasal washing samples were obtained under a short-term
799 isoflurane inhalation anesthesia from individual hamsters by administering 200 μ l PBS to
800 each nostril and collecting the reflux. Animals were sampled daily from 1 dpi to 9 dpi and
801 afterwards every second day until 21 dpi. Under euthanasia, serum samples and an organ
802 panel comprising representative upper (URT) and lower respiratory tract (LRT) tissues were
803 collected from each hamster. All animals were checked daily for signs of clinical disease and
804 weight loss. Animals reaching the humane endpoint, e.g., falling below 80% of the initial
805 body weight relative to 0 dpi, were humanely euthanized.

806

807 **Ferret competition studies**

808 The study outline for the ferret competition studies can be seen in Extended Data Figure 2b.
809 Similar to the hamster study, 12 ferrets (six donor ferrets and six contact ferrets) from the FLI
810 in-house breeding were housed pairwise in strictly separated cages to prevent spillover
811 contamination. Of these, six ferrets were intranasally inoculated with an equal 250 μ l mixture
812 of SARS-CoV-2 Alpha and Delta or Delta and Omicron-BA.1. The inoculum of the mixture
813 as well as from the single viruses was back titrated and the ratio of each variant was
814 determined by dividing the TCID₅₀/mL values of single VOC1 by VOC2. Ferret pairs were
815 separated for the first 24 hours following inoculation. Subsequently, the ferrets were co-
816 housed again, allowing direct contact of donor to contact ferrets. All ferrets were sampled via
817 nasal washings with 750 μ l PBS per nostril under a short-term isoflurane inhalation
818 anesthesia. All ferrets, which were in the study group on the respective days, were sampled
819 daily until 8 dpi and afterwards every second day until the animals were negative for SARS-

820 CoV-2 viral genome in RT-qPCR and one last time at the study end (21 dpi). Physical
821 condition of all animals was monitored daily throughout the experiment.

822

823 **Ferret single infection studies**

824 The study outline for the ferret single infection studies can be seen in Extended Figure 2c. 12
825 ferrets (nine donor and three contact animals) from the FLI in-house breeding were housed in
826 multiple connected cage units. The donor ferrets were inoculated either with 250 µl of SARS-
827 CoV-2 Delta ($10^{4.8125}$ TCID₅₀/ferret, calculated from back-titration of the original material) or
828 Omicron-BA.1 ($10^{5.125}$ TCID₅₀/ferret, calculated from back-titration of the original material)
829 in two separate and independent animal trials. Contact animals were separated from the donor
830 animals for the first 24 hours, followed by co-housing again to allow direct contact of donor
831 and contact animals. All ferrets were sampled via nasal washings with 750 µl PBS per nostril
832 under a short-term isoflurane inhalation anesthesia. Sampling was done daily until 8 dpi and
833 afterwards every second day until the study end at 14 dpi. For serological analysis, serum was
834 collected at the study end (14 dpi). Physical condition of all animals was monitored daily
835 throughout the experiment. For analysis of SARS-CoV-2 Omicron-BA.1 viral genome
836 distribution in LRT and URT, six ferrets from the respective Omicron-BA.1-single infection
837 trial were euthanized at 6 dpi and viral organ load was determined via Omicron-BA.1-specific
838 RT-qPCR.

839

840 **Mouse studies**

841 hACE2-KI mice (B6.Cg-*Ace2*^{tm1(ACE2)Dwnt}) and hACE2-K18Tg mice (Tg(K18-
842 hACE2)2Prlmn) were described previously^{9,21}. All mice were bred at the specific pathogen-
843 free facility of the Institute of Virology and Immunology and housed as previously described

844 ¹⁰. Mice were anesthetized with isoflurane and inoculated intranasally with 20 μ l per nostril.
845 For single-infection experiments, 7- to 17-week-old male mice were inoculated with a dose of
846 2×10^4 TCD₅₀/mouse of either Delta (EPI_ISL_2535433) or Omicron-BA.1
847 (EPI_ISL_7062525) isolates. For competition experiments, 7 to 19-week-old female mice
848 were inoculated with a mixture inoculum containing the Delta and Omicron-BA.1 isolates or
849 a mixture of the recombinant spike clones SARS-CoV-2^{S-Omicron} and SARS-CoV-2^{S-Delta}.
850 Inoculum mixtures were generated by mixing the respective viruses aiming at a 1:1 ratio
851 based TCID₅₀/mL titers of the single virus. The ratio of each variant in the prepared inocula
852 was further determined by standard RT-qPCR. At 2 or 4 dpi, mice were euthanized and
853 organs were aseptically dissected. Systematic tissue sampling was performed as described
854 previously ⁹.

855 K18-hACE2 mice (all female, 7 to 15 weeks old) were immunized intramuscularly with a
856 single dose of 1 μ g of mRNA-Vaccine Spikevax (Moderna). Five weeks after immunization,
857 the immunized mice and a group of sex- and age-matched naïve animals were challenged
858 intranasally with 20 μ l per nostril with the virus inoculum described in the results section.
859 Euthanasia and organ collection was performed 2 or 6 dpi as described above.

860 All mice were monitored daily for body weight loss and clinical signs. Oropharyngeal swabs
861 were collected daily as described before¹⁰.

862

863 **Animal specimens work up, viral RNA detection and quantification**

864 Organ samples of about 0,1 cm³ size from ferrets and hamsters were homogenized in a 1 mL
865 mixture composed of equal volumes of Hank's balanced salts MEM and Earle's balanced
866 salts MEM containing 2 mM L-glutamine, 850 mg l⁻¹ NaHCO₃, 120 mg l⁻¹ sodium
867 pyruvate, and 1% penicillin-streptomycin) at 300 Hz for 2 min using a Tissuelyser II
868 (Qiagen) and were then centrifuged to clarify the supernatant. Organ samples from mice were

869 either homogenized in 0.5 mL of RA1 lysis buffer supplemented with 1% β -mercaptoethanol
870 as described¹⁰.

871 Nucleic acid was extracted from 100 μ l of the nasal washes after a short centrifugation step or
872 100 μ l of organ sample supernatant using the NucleoMag Vet kit (Macherey Nagel). Nasal
873 washings, oropharyngeal swabs and organ samples were tested by virus-variant specific RT-
874 qPCR to analyze the genomic ratio of the two different viruses used for inoculation.

875 Three specific RT-qPCR assays for SARS-CoV-2 Alpha, Delta and Omicron-BA.1 were
876 designed based on the specific genome deletions within the ORF1 and S gene (Supplementary
877 Information Table 4). Here, virus specific primers were used to achieve a high analytical
878 sensitivity (less than 10 genome copies/ μ l template) of the according PCR assays, also in
879 samples with a high genome load of the non-matching virus. For each specific RT-qPCR a
880 dilution row of a standard with known concentration determined by digital droplet PCR was
881 carried along to calculate the viral genome copy number per mL.

882 The RT-qPCR reaction was prepared using the qScript XLT One-Step RT-qPCR ToughMix
883 (QuantaBio, Beverly, MA, USA) in a volume of 12.5 μ l including 1 μ l of the respective FAM
884 mix and 2.5 μ l of extracted RNA. The reaction was performed for 10 min at 50°C for reverse
885 transcription, 1 min at 95°C for activation, and 42 cycles of 10 sec at 95°C for denaturation,
886 10 sec at 60°C for annealing and 20 sec at 68°C for elongation for the Omicron-BA.1-
887 detecting assay. For detection of Alpha and Delta, the following thermal profile was applied:
888 10 min at 50°C for reverse transcription, 1 min at 95°C for activation, and 42 cycles of 5 sec
889 at 95°C for denaturation, 5sec at 62°C for annealing and 10 sec at 68°C for elongation.
890 Fluorescence was measured during the annealing phase. RT-qPCRs were performed on a
891 BioRad real-time CFX96 detection system (Bio-Rad, Hercules, USA).

892

893 **Histopathological and immunohistochemical analysis**

894 The left lung and the left hemisphere of the brain from K18-hACE2 mice were collected upon
895 necropsy and immersed in 10% neutral-buffered formalin. Following fixation, both tissues
896 were embedded in paraffin, cut at 4 μ m and stained with hematoxylin and eosin (H&E) for
897 histological evaluation. Lung tissue pathology was scored according to a previously published
898 scoring scheme¹⁰. A 1:3000 dilution of a rabbit polyclonal anti-SARS-CoV nucleocapsid
899 antibody (Rockland, 200-401-A50) was used for the immunohistochemical (IHC) analysis of
900 the lung and the brain. Paraffin blocks were cut at 3 μ m, placed in a BOND
901 RX^m immunostainer (Leica Byosystems, Germany) and were incubated for 30 minutes with
902 the first antibody at room temperature. Antigen retrieval was performed by incubating the
903 slides with a citrate buffer for 30 min at 100°C. BondTM Polymer Refine Detection
904 visualisation kit (Leica Byosystems, Germany) was afterwards used for signal detection using
905 DAB as chromogen and counterstaining with hematoxylin.

906

907 **Serological tests**

908 To evaluate the virus neutralizing potential of serum samples, we performed a live virus
909 neutralization test following an established standard protocol as described before. Briefly, sera
910 were prediluted 1/16 in MEM and further diluted in log2 steps until a final tested dilution of
911 1/4096. Each dilution was evaluated for its potential to prevent 100 TCID₅₀ SARS-CoV-
912 2/well of the respective VOC from inducing cytopathic effect in Vero E6 cells, giving the
913 virus neutralization titer (VNT₁₀₀). Additionally, serum samples were tested by multispecies
914 ELISA for sero-reactivity against the SARS-CoV-2 RBD domain²².

915

916 **Human precision-cut lung slice cultures**

917 The generation of PCLSs was done as described previously with some adaptations to human
918 specimens ²³. Control lung tissue (preserved pulmonary architecture without emphysema or
919 inflammation) was obtained from the distal non-tumorous areas of lung resections. Prior to
920 processing, lung tissue was tested for SARS-CoV-2 by qPCR. After gathering, control lung
921 tissue was maintained in DMEM (ThermoFisher), supplemented with 1X ITS (Sigma) until
922 further processing 2 to 5 hours later. Next, lung tissue specimens were washed with PBS
923 (ThermoFisher) containing 1X Antibiotic-Antimycotic (ThermoFisher), infused with 2% low-
924 melting point agarose (Sigma) in DMEM, and subsequently put into cold PBS at 4°C for 15
925 min to allow the agarose to solidify. Next, the perfused tissue was cut into small cubes of
926 approximately 1 cm³, placed in the specimen tube and embedded in 2% low-melting point
927 agarose. To generate PCLSs with a thickness of 400 µm, an automated Compresstome VF-
928 310-0Z Vibrating Microtome (Precisionary) was used following the recommended
929 parameters: speed of 8 mm/sec and oscillation of 27 Hz. The slices were transferred into a 12-
930 well plate (one PCLS per well) with culture medium (DMEM, supplemented with 1% FBS,
931 100 units/mL of penicillin and 100 µg/mL streptomycin, and 2.5 µg/mL of Amphotericin B
932 (all from ThermoFisher). Cultures were maintained at 37°C, 5% CO₂ and culture medium was
933 changed every 24 h for 2-3 days prior infection.

934

935 **Infection of human precision-cut lung slice cultures**

936 PCLS cultures were infected with a 1:1 mixture of SARS-CoV-2^{S-Delta} and SARS-CoV-2^{S-}
937 ^{Omicron} in 0.5 mL DMEM, supplemented with 0.1% FBS, 100 units/mL of penicillin and 100
938 µg/mL streptomycin, and 2.5 µg/mL of Amphotericin B for 2-4 hours. Next, the inoculum
939 was removed, PCLSs were washed twice with pre-warmed PBS, and 2 mL of culture medium
940 were added per well. Medium was changed after 24 h. 48 hpi, PCLSs were washed and

941 transferred into cold TRIzol reagent (ThermoFisher) and kept at -70°C until further
942 processing.

943

944 **RNA isolation of human precision-cut lung slice (PCLS) cultures**

945 Total RNA was extracted from PCLS cultures using TRIzol reagent in combination with the
946 RNA Clean & Concentrator Kit (Zymo Research). Briefly, Tissue slices were homogenized
947 using MagNA Lyser Green Beads (Roche diagnostics) in combination with a tissue
948 homogenizer (MP Biomedicals) and lysed with 700 µl of cold TRIzol reagent per PCLS. Two
949 hundred mL of chloroform was added to the TRIzol lysate, the samples were mixed
950 vigorously, and then incubated for 2-3 min at room temperature. Next, the extractions were
951 centrifuged at 12'000 g for 15 min at 4°C. The aqueous phase was then collected, mixed 1:1
952 with 75% ethanol, and incubated for 10 min at room temperature to let RNA precipitate. The
953 RNA precipitate was further purified with the RNA Clean & Concentrator Kit according to
954 the manufacturer's instructions.

955

956 **Well-differentiated primary nasal and bronchial epithelial cells**

957 Primary human nasal epithelial cell cultures (hNECs) were obtained commercially (Epithelix
958 Sàrl) and primary human bronchial epithelial cell cultures (hBECs) were isolated from lung
959 explants. The generation of well-differentiated (WD)-hNECs and WD-hBECs at the air-liquid
960 interface (ALI) was described previously with minor adjustments²⁴. For expansion, hNECs
961 and hBECs were cultured in collagen-coated (Sigma) cell culture flasks (Costar) in
962 PneumaCult Ex Plus medium, supplemented with 1 µM hydrocortisone, 5 µM Y-27632 (Stem
963 Cell Technologies), 1 µM A-83-01 (Tocris), 3 µM isoproterenol (abcam), and 100 µg/mL
964 primocin (Invivogen) and maintained in a humidified atmosphere at 37°C, 5% CO₂. Next, the

965 expanded cells were seeded at a density of 50'000 cells per insert onto collagen-coated
966 (Sigma) 24-well plate inserts with a pore size of 0.4 μm (Greiner Bio-One) and grown under
967 submerged conditions with 200 μl of supplemented PneumaCult ExPlus medium on the apical
968 side and 500 μl in the basolateral chamber. When cells reached confluence, as assessed by
969 measuring the trans-epithelial electrical resistance (TEER) using a Volt/Ohm Meter
970 (EVOM²/STX2, World Precision Instruments) and microscopical evaluation, the apical
971 medium was removed, cells were washed with pre-warmed Hank's balanced salt solution
972 (HBSS, ThermoFisher), and then exposed to the air. PneumaCult ALI medium supplemented
973 with 4 $\mu\text{g}/\text{mL}$ heparin (Stem Cell Technologies), 5 μM hydrocortisone, and 100 $\mu\text{g}/\text{mL}$
974 primocin was added to the basolateral chamber to induce differentiation of the cells. Every 2-
975 3 days, the basal medium was changed and cultures were maintained at 37°C, 5% CO₂ until
976 the appearance of ciliated cells and mucus production. The cell layer was washed once a week
977 with 250 μL of pre-warmed HBSS for 20 min at 37°C to get rid of mucus. The hNEC and
978 hBEC cultures were considered well-differentiated 3 weeks post-exposure to ALI.

979

980 **Statistical analysis**

981 Statistical analysis was performed using GraphPad Prism 8. Unless noted otherwise, the
982 results are expressed as mean \pm s.d. Specific tests are indicated in the main text or the figure
983 legends.

984

985 **References**

986 18 van den Worm, S. H. *et al.* Reverse genetics of SARS-related coronavirus using
987 vaccinia virus-based recombination. *PLoS One* 7, e32857,
988 doi:10.1371/journal.pone.0032857
989 PONE-D-11-21011 [pii] (2012).

990 19 Kaleta, T. *et al.* Antibody escape and global spread of SARS-CoV-2 lineage A.27. *Nat Commun* **13**, 1152, doi:10.1038/s41467-022-28766-y (2022).

991

992 20 Thi Nhu Thao, T. *et al.* Rapid reconstruction of SARS-CoV-2 using a synthetic genomics platform. *Nature* **582**, 561-565, doi:10.1038/s41586-020-2294-9

993

994 10.1038/s41586-020-2294-9 [pii] (2020).

995 21 McCray, P. B., Jr. *et al.* Lethal infection of K18-hACE2 mice infected with severe acute respiratory syndrome coronavirus. *J Virol* **81**, 813-821, doi:JVI.02012-06 [pii]

996

997 10.1128/JVI.02012-06 (2007).

998 22 Wernike, K. *et al.* Multi-species ELISA for the detection of antibodies against SARS-CoV-2 in animals. *Transbound Emerg Dis* **68**, 1779-1785, doi:10.1111/tbed.13926

999

1000 (2021).

1001 23 Brügger, M. *et al.* Pulmonary mesenchymal stem cells are engaged in distinct steps of host response to respiratory syncytial virus infection. *PLoS Pathog* **17**, e1009789,

1002

1003 doi:10.1371/journal.ppat.1009789

1004 PPATHOGENS-D-21-00450 [pii] (2021).

1005 24 Fahmi, A. *et al.* SARS-CoV-2 can infect and propagate in human placenta explants.

1006 *Cell Rep Med* **2**, 100456, doi:10.1016/j.xcrm.2021.100456

1007 S2666-3791(21)00324-4 [pii] (2021).

1008 25 Tyson, J. R. *et al.* Improvements to the ARTIC multiplex PCR method for SARS-CoV-2 genome sequencing using nanopore. *bioRxiv*, 2020.2009.2004.283077,

1009

1010 doi:10.1101/2020.09.04.283077 (2020).

1011

1012

1014 **Extended Data Figure legends**

1015 **Extended Data Fig. 1: Sequencing data analysis.** **a)** Schematic illustrating the general
1016 sequencing and bioinformatics workflow used to determine the virus ratios in Fig. 1e-g. For
1017 each virus mixture in the NEC, BEC, and lung explants samples RNA was extracted from
1018 apical washes at 2 and/or 6 dpi and sequenced on the MinION sequencer using a modified
1019 version of the ARTIC protocol for SARS-CoV-2 sequencing (1200 bp amplicons with the
1020 midnight primer scheme, see methods for specific modifications)²⁵. Live GPU basecalling
1021 was performed using Guppy v.5.1.15 (Oxford Nanopore technologies) in high-accuracy mode
1022 and the downstream analysis was performed using a modified version of the ARTIC
1023 bioinformatics pipeline (<https://artic.network/ncov-2019/ncov2019-bioinformatics-sop.html>).
1024 Briefly, input reads were filtered based on read length and then mapped to the Wuhan-Hu-1
1025 reference genome (accession MN908947.3) using the ‘artic minion’ command. BAM
1026 alignment files from the ARTIC pipeline were then used for variant calling in longshot
1027 (v.0.4.4) with an input VCF file containing VOC Delta and Omicron-BA.1 mutations
1028 provided in order to call variants at specific nucleotide sites. The downstream analysis of VCF
1029 files was performed in R v.4.1.3 and involved filtering the VCF file for each sample to
1030 exclude mutations shared between both viruses in the mixture (shared, blue), non-lineage-
1031 defining mutations (non-LDM, grey), and any sites with overlapping mutations in both
1032 viruses that were difficult to call (other, green). Mutations called with a depth of coverage
1033 lower than 100 were also excluded from the downstream analysis (bottom left panel).
1034 Mutations in filtered VCF files (bottom middle panel) were then used to calculate the mean
1035 mutation frequency for each virus per sample. Finally, the mean \pm sd virus ratio was
1036 calculated for each time point (bottom right panel). **b)** Stacked bar plot showing the frequency
1037 of individual mutations called in the VCF file for the WT-614G and Omicron inoculum
1038 before (top) and after (bottom) filtering. **c)** Stacked bar plot showing the frequency of

1039 individual mutations in the filtered VCF files for all WT-614G and Omicron NEC samples (3
1040 donors, 2 and 6 dpi). These values were used to calculate a mean mutation frequency for each
1041 virus per sample, which is shown in **d**).

1042

1043 **Extended Data Fig. 2: Experimental outline for studies with Syrian hamsters and**
1044 **ferrets.** Donor hamsters (n=6) were intranasally inoculated with either an Omicron-BA.1, -
1045 Delta or an Alpha-Delta mixture at iso-titer. A Competition studies in hamsters. Each donor
1046 was co-housed with one contact I hamster 1dpi. 4dpi after euthanasia of the donors, one
1047 contact II hamster was introduced to each contact I hamster. B Study outline for the ferret
1048 competition studies with Omicron-BA.1-Delta and Alpha-Delta mixtures. C Timeline for the
1049 ferret study with single-variant-inocula (either Omicron-BA.1 or Delta). 6dpi six donor
1050 animals, which were inoculated with Omicron-BA.1, were euthanized for determination of
1051 viral organ load in URT and LRT.

1052

1053 **Extended Data Fig. 3: Body weight changes and survival rate of hamsters/ferrets in the**
1054 **competitive infection and transmission experiments. a)** Survival of Syrian hamsters during
1055 competitive infection and transmission experiment between Alpha and Delta VOC. **b)**
1056 Survival of Syrian hamsters during competitive infection and transmission experiment
1057 between Delta and Omicron-BA.1 VOC. **c)** Percentages of body weight change in Syrian
1058 hamsters competitively inoculated with Alpha and Delta VOC. **d)** Percentages of body weight
1059 change in Syrian hamsters competitively inoculated with Delta and Omicron-BA.1 VOC. **e)**
1060 Percentages of body weight change in ferrets during single infection study with Delta VOC. **f)**
1061 Percentages of body weight change in ferrets during single infection study with Omicron-
1062 BA.1 VOC. Red star and arrow show timepoint of euthanasia (6 dpi) for six ferrets to analyze
1063 viral load distribution in organs. **g)** Percentages of body weight change in ferrets

1064 competitively inoculated with Alpha and Delta VOC. **h)** Percentages of body weight change
1065 in ferrets competitively inoculated with Delta and Omicron-BA.1 VOC.

1066
1067 **Extended Data Fig. 4: Viral load in organs of Contact I and Contact II hamsters**
1068 **competitively inoculated with Delta and Omicron-BA.1 VOC at respective euthanasia**
1069 **timepoints** Viral genome load in upper (URT) and lower (LRT) respiratory tract tissues of
1070 Syrian hamsters in the competitive transmission experiment between SARS-CoV-2 VOCs
1071 Delta and Omicron-BA.1. Syrian hamsters were inoculated with comparable genome
1072 equivalent mixture of Delta and Omicron-BA.1 VOC. Absolute quantification was performed
1073 by RT-qPCR analysis of tissue homogenates of Contact I and Contact II hamsters in relation
1074 to a set of defined standards. Tissue samples were collected at euthanasia (Euth.). Pie chart
1075 colors illustrate the ratio of variants detected in each sample at the indicated dpi or days post
1076 contact (dpc). Pie chart sizes are proportional to the total viral genome copies reported above.
1077 Grey pies indicate values below the LOD (<10³ viral genome copies per mL).

1078
1079 **Extended Data Fig. 5: Competitive infection of hamsters with SARS-CoV-2 Delta and**
1080 **Alpha** Six donor hamsters were each inoculated intranasally with 10^{4.625} TCID₅₀ determined
1081 by back titration and composed of a mixture of SARS-CoV-2 Alpha (dark blue) and Delta
1082 (purple) at 1.95:1 ratio determined by back-titration of the original single virus amounts used
1083 in the experiment. Donor hamsters, contact I and II hamsters were co-housed sequentially as
1084 shown in Extended Data Fig.. 2. Nasal washings were performed daily from 1-9 dpi and
1085 afterwards every two days until 21 dpi. Each pie chart illustrates the ratio of the respective
1086 viruses in nasal washings for each sampling day. Total genome copies/mL are indicated
1087 above or below the respective pies. Hamster silhouettes are colored according to the dominant

1088 variant (>66%) detected in the latest sample of each animal. Black crosses indicate the
1089 respective animal was already dead.

1090

1091 **Extended Data Fig. 6: Competitive infection of ferrets with SARS-CoV-2 Alpha and**
1092 **Delta** Six donor ferrets were each inoculated with 10^5 TCID₅₀ determined by back titration
1093 and composed of a mixture of Alpha (dark blue) and SARS-CoV-2 Delta (purple) at a 1.33:1
1094 ratio determined by back-titration of the original single virus amounts used in the experiment.
1095 Donor and Contact ferrets were co-housed sequentially as shown in Extended Data Fig.. 2. Pie
1096 charts illustrate the ratio of either SARS-CoV-2 Alpha or SARS-CoV-2 Delta detected in
1097 nasal washings of the donor or contact ferrets in the respective ferret groups at indicated dpi.
1098 Viral genome copies/mL are shown above or below respective pie charts; Grey pies indicate
1099 values below the LOD (<10³ viral genome copies per mL). Coloring of the ferret silhouettes
1100 refers to the predominant SARS-CoV-2 variant (>66%) detected in the latest sample of the
1101 respective animal.

1102

1103 **Extended Data Fig. 7: ELISA and VNT₁₀₀ of sera received from competitive infection**
1104 **experiments with Alpha and Delta in hamsters/ferrets** Blue dots represent neutralization of
1105 Alpha variant, purple dots represent neutralization of the Delta variant in the respective
1106 animal according to the highest dilution where virus neutralization was visible (left Y-Axis).
1107 Black dots shows RBD-ELISA-reactivity of animal sera at respective euthanasia timepoint
1108 (right Y-Axis) **(a)** VNT₁₀₀ and RBD-ELISA from animal sera of the Alpha vs Delta
1109 competitive infection and transmission experiment in hamsters **(b)** VNT₁₀₀ and RBD-ELISA
1110 from animal sera of the competitive infection and transmission experiment with Delta and
1111 Alpha VOC in ferrets.

1112

1113 **Extended Data Fig. 8: Viral load in organs of Donor, Contact I and Contact II hamsters**
1114 **competitively inoculated with Alpha and Delta VOC at respective euthanasia timepoints**

1115 Viral genome load in upper (URT) and lower (LRT) respiratory tract tissues of Syrian
1116 hamsters in the competitive transmission experiment between SARS-CoV-2 VOCs Alpha and
1117 Delta. Syrian hamsters were inoculated with comparable genome equivalent mixture of either
1118 Alpha and Delta VOC. Absolute quantification was performed by RT-qPCR analysis of tissue
1119 homogenates of donor, contact I and contact II hamsters in relation to a set of defined
1120 standards. Tissue samples were collected at euthanasia (Euth.). Pie chart colors illustrate the
1121 ratio of variants detected in each sample at the indicated dpi or days post contact (dpc). Pie
1122 chart sizes are proportional to the total viral genome copies reported above. Grey pies indicate
1123 values below the LOD (<10³ viral genome copies per mL).

1124

1125 **Extended Data Fig. 9: Delta spike mutations drive enhanced fitness in humanized mice.**
1126 **a)** hACE2-KI mice (7 to 16 week-old male) were intranasally inoculated with 10^{4.3} tissue
1127 culture infectious dose 50 (TCID₅₀) of Delta or Omicron isolates. The left graph reports the
1128 body weight loss for each of the hACE2-KI in Fig. 3a. The right graph depicts the viral copies
1129 in brain and olfactory bulb samples quantified using E-gene probe-specific RT-qPCR. Data
1130 are mean±s.d. from the indicated number of biological replicates from a single experiment.
1131 Statistical significance was determined using an unpaired Student t-test; **P<0.01. **b)**
1132 hACE2-KI mice (7 to 19 week-old female, n=6/group) were intranasally inoculated with 10⁴
1133 TCID₅₀ of a 1:1 mix of Delta and Omicron or SARS-CoV-2^{S-Delta} and SARS-CoV-2^{S-Omicron}.
1134 The graph on the left shows the body weight loss for each of the inoculated animal. The graph
1135 on the right shows the histopathological score in these mice. Data are mean±s.d. from the
1136 indicated number of biological replicates from a single experiment.

1137

1138 **Extended Data Fig. 10: mRNA vaccine induced reduction in replication and**
1139 **pathogenesis of SARS-CoV-2 clones in K18-hACE2 transgenic mice. a)** Female K18-
1140 hACE2 transgenic mice (7 to 15 weeks old) were immunized intramuscularly with a single
1141 dose of 1 μ g of mRNA-Vaccine Spikevax (Moderna). After two weeks the neutralizing
1142 antibody titers against SARS-CoV-2 SARS-CoV-2^{614G} determined. Later, mice were
1143 intranasally inoculated with 10^4 tissue culture infectious dose 50 (TCID₅₀) of SARS-CoV-
1144 2^{614G}, SARS-CoV-2^{S-Delta} and SARS-CoV-2^{S-Omicron}. **b)** The clinical scores of the mice were
1145 monitored daily. **c)** Oropharyngeal swabs, lung, nose, brain and olfactory bulb samples of the
1146 infected mice were collected at 2 or 6 days post-infection (dpi) to determine the viral load
1147 (n = 4 for each virus). Histopathological scores were given to evaluate the severity of the lung
1148 pathology. **d)** Viral RNA-dependent RNA polymerase (RdRp) gene copies of brain and
1149 olfactory bulb tissues were quantified using probe-specific RT-qPCR. **e)** Infectious virus
1150 titers from the brain samples were determined using TCID₅₀ assays in VeroE6-TMPRSS2
1151 cells. **f)** Virus neutralization capacities of the serum collected from infected mice at 6 dpi are
1152 tested against SARS-CoV-2^{S-Delta} and SARS-CoV-2^{S-Omicron} clones. The color key in b also
1153 applies to c, d, e and f. Statistical significance was determined using two-way ANOVA (a-d)
1154 and P values were adjusted using Tukey's multiple-comparison test; *P < 0.05, **P < 0.01,
1155 ***P < 0.001, ****P < 0.0001. Data were obtained from one experiment. Each data point
1156 represents one biological replicate.

1157

1158 **Extended Data Table 1:** List of viruses used in this study.

Figure 1

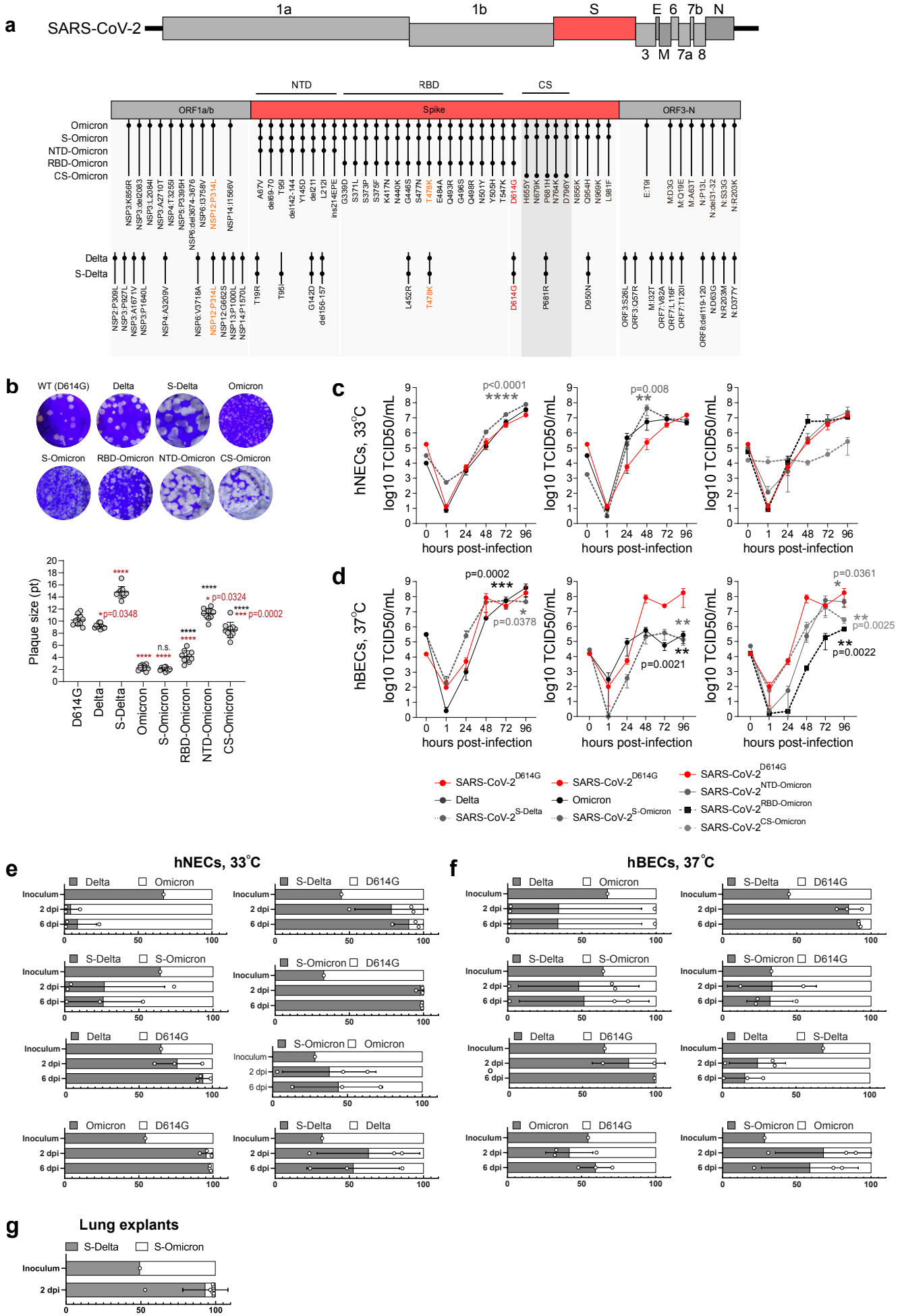


Figure 2

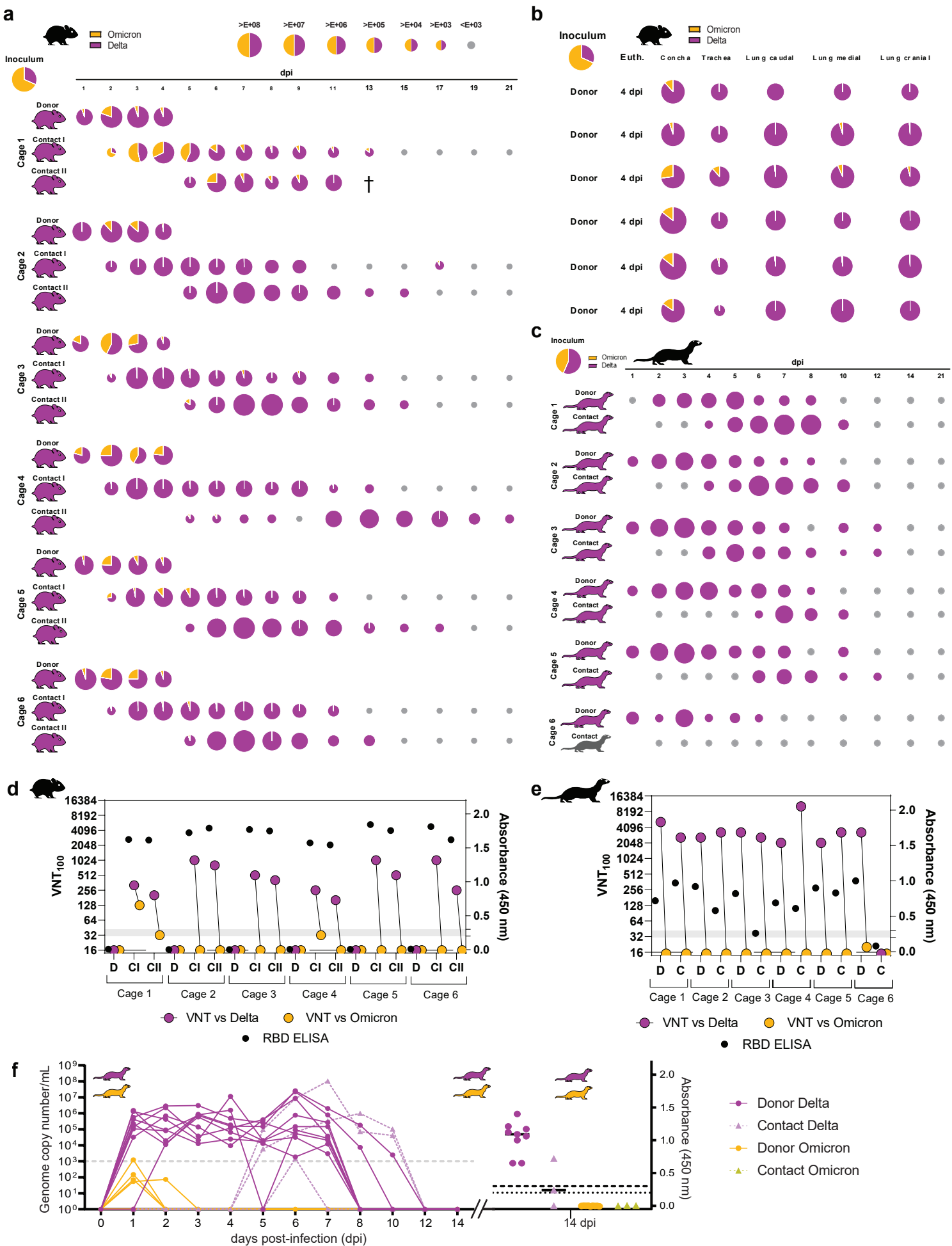


Figure 3

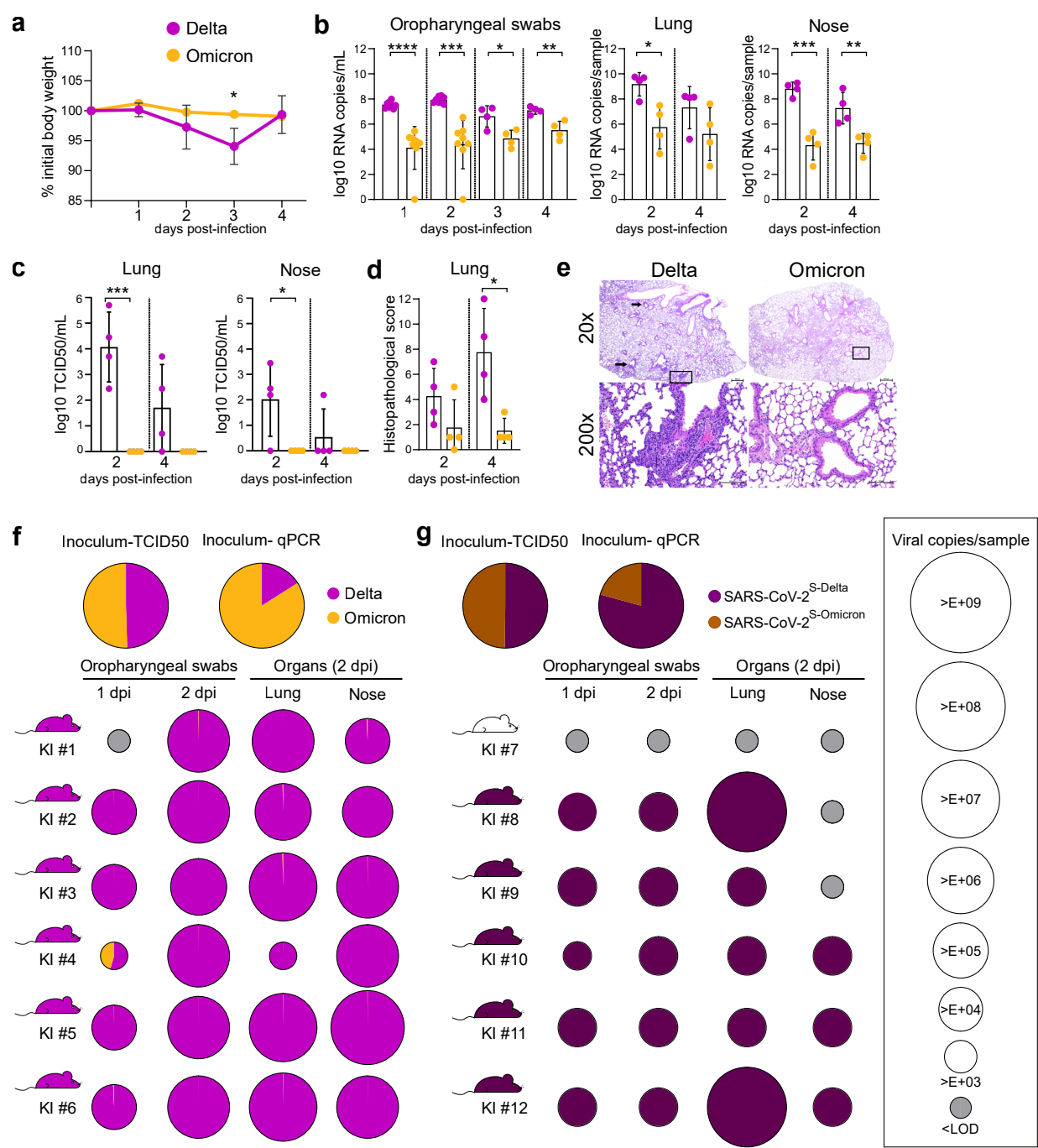
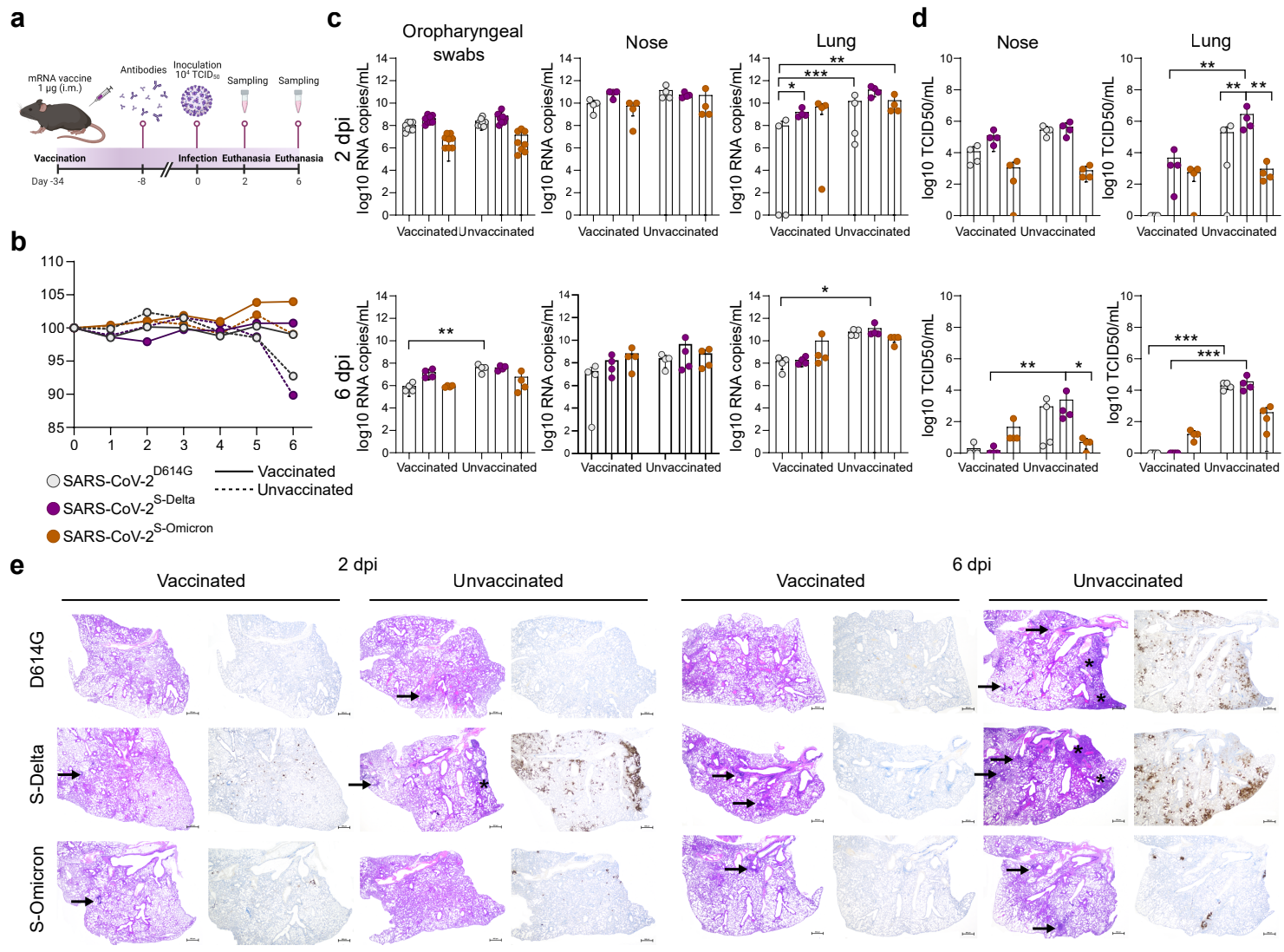
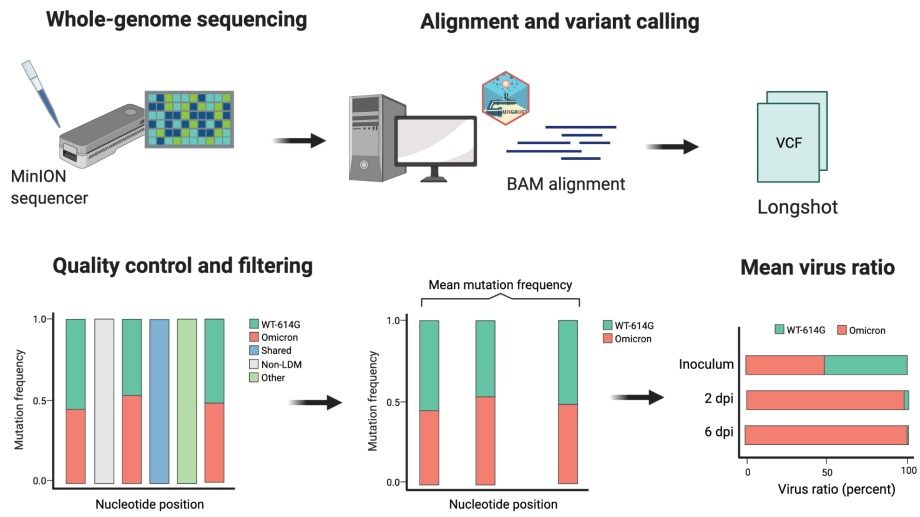


Figure 4

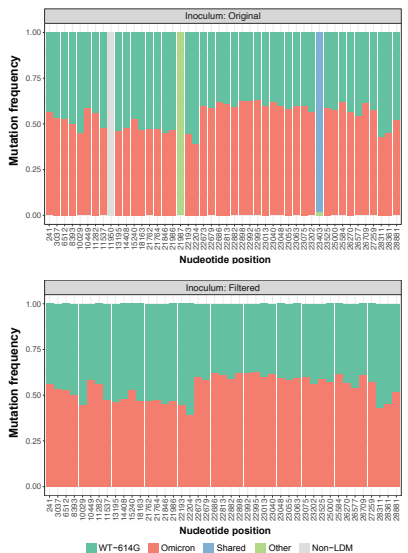


Extended Data Figure 1

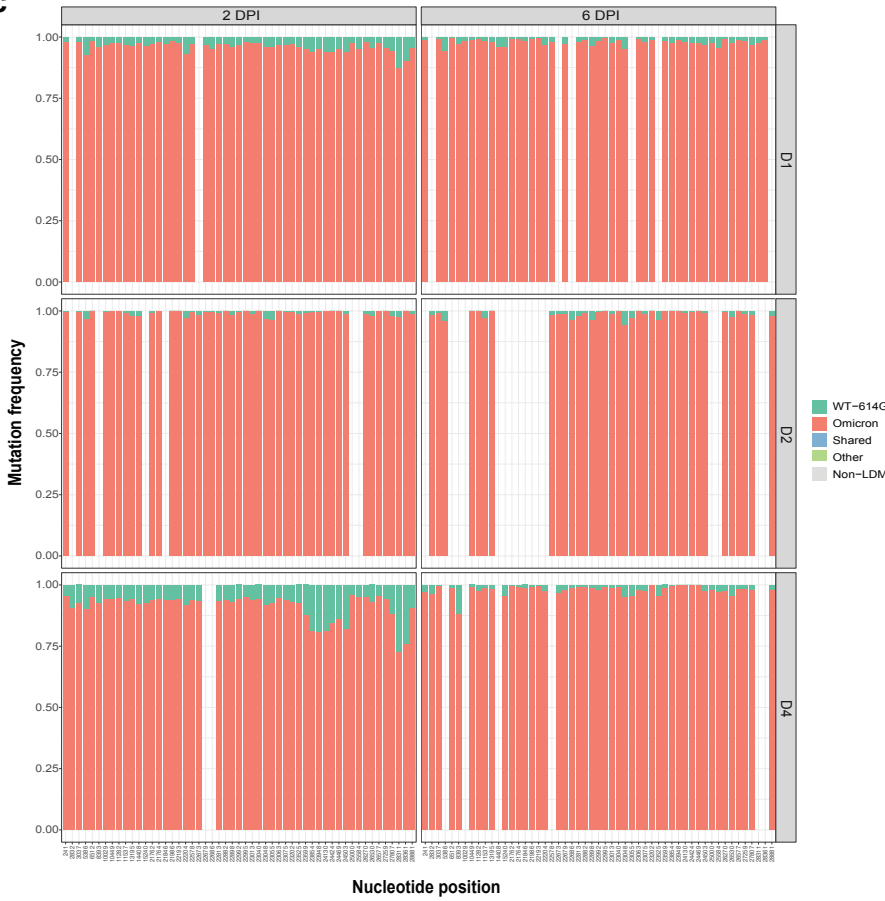
a



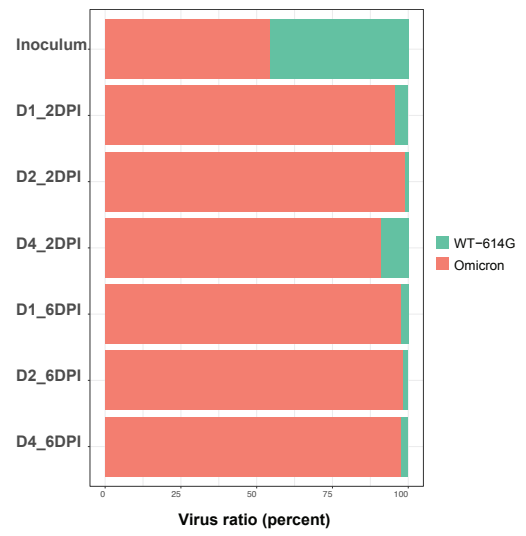
b



c

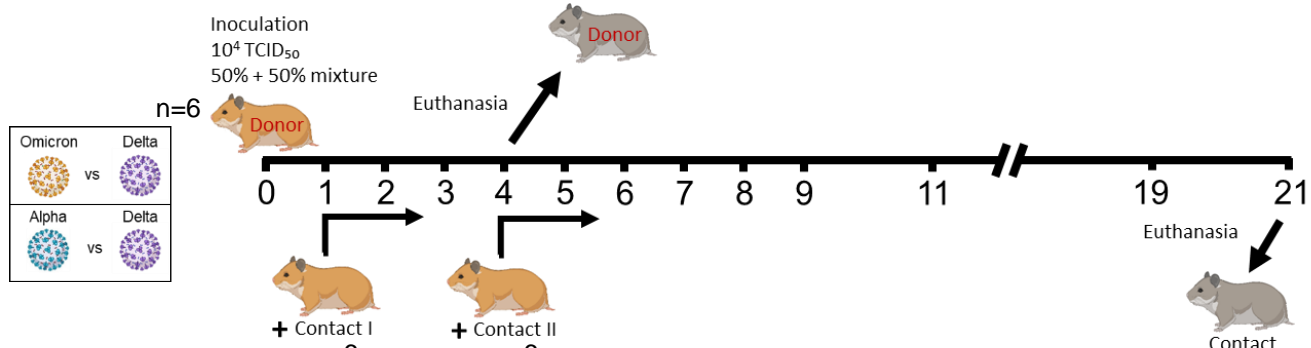


d

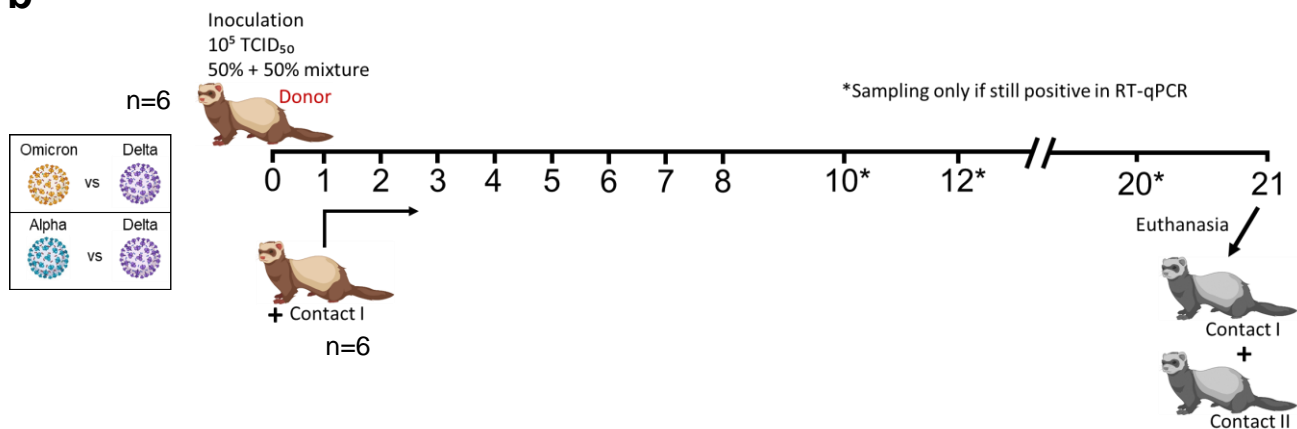


Extended Data Figure 2

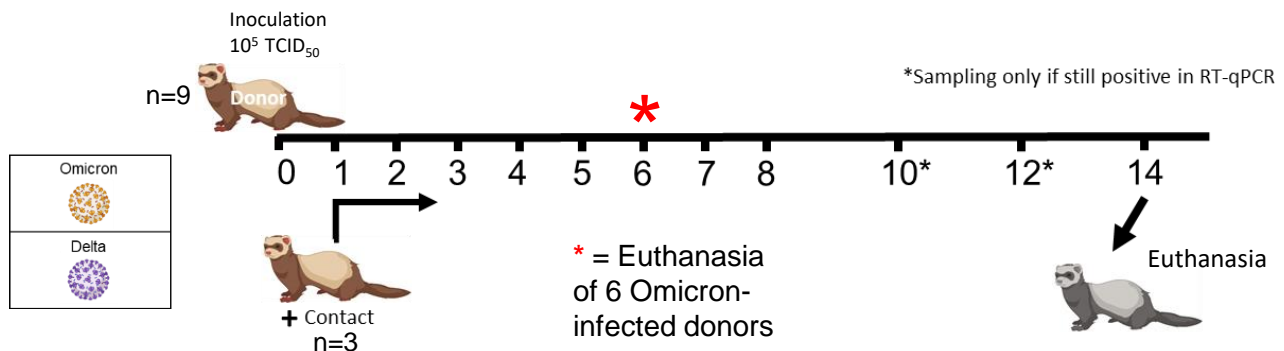
a



b



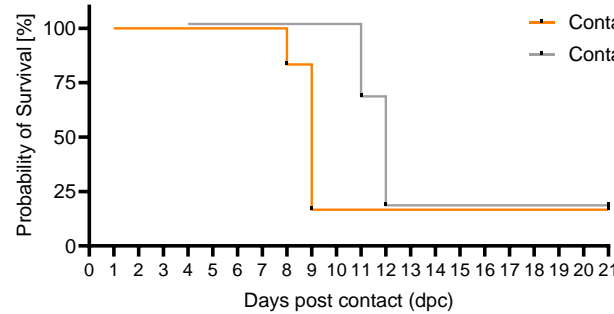
c



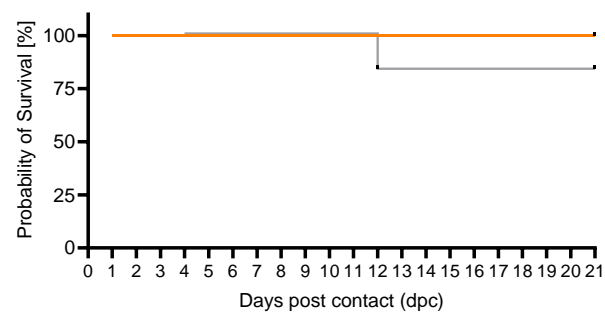
Extended Data Figure 3



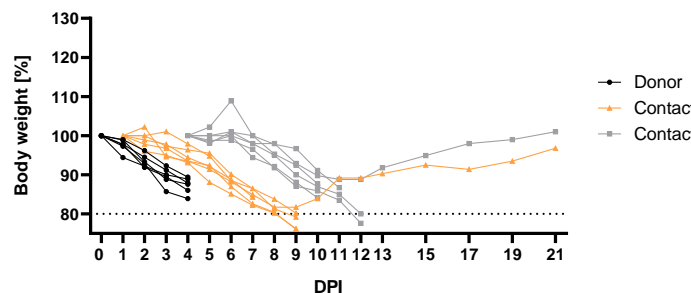
Contact I
Contact II



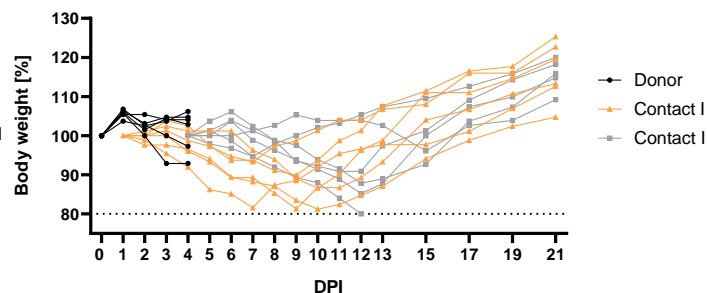
Contact I
Contact II



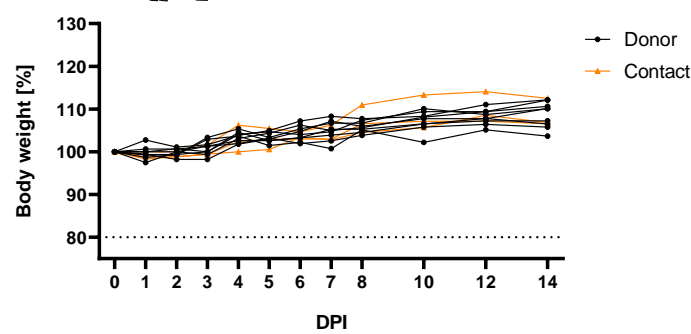
Donor
Contact I
Contact II



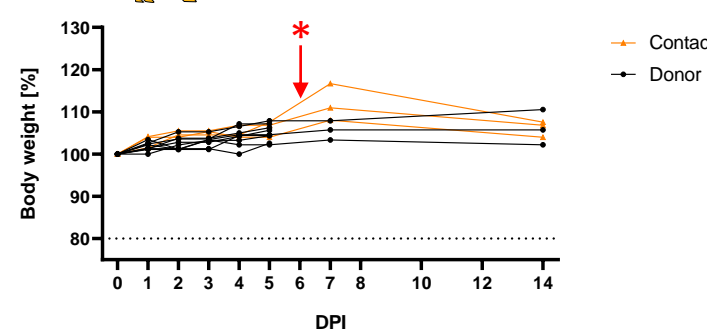
Donor
Contact I
Contact II



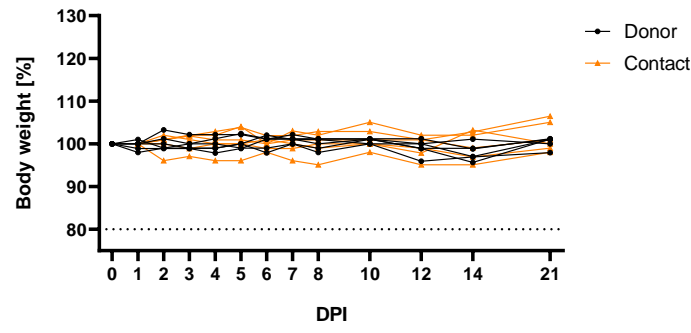
Donor
Contact



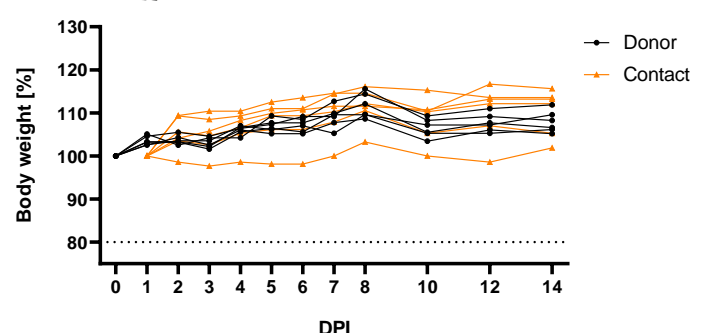
Contact
Donor



Donor
Contact

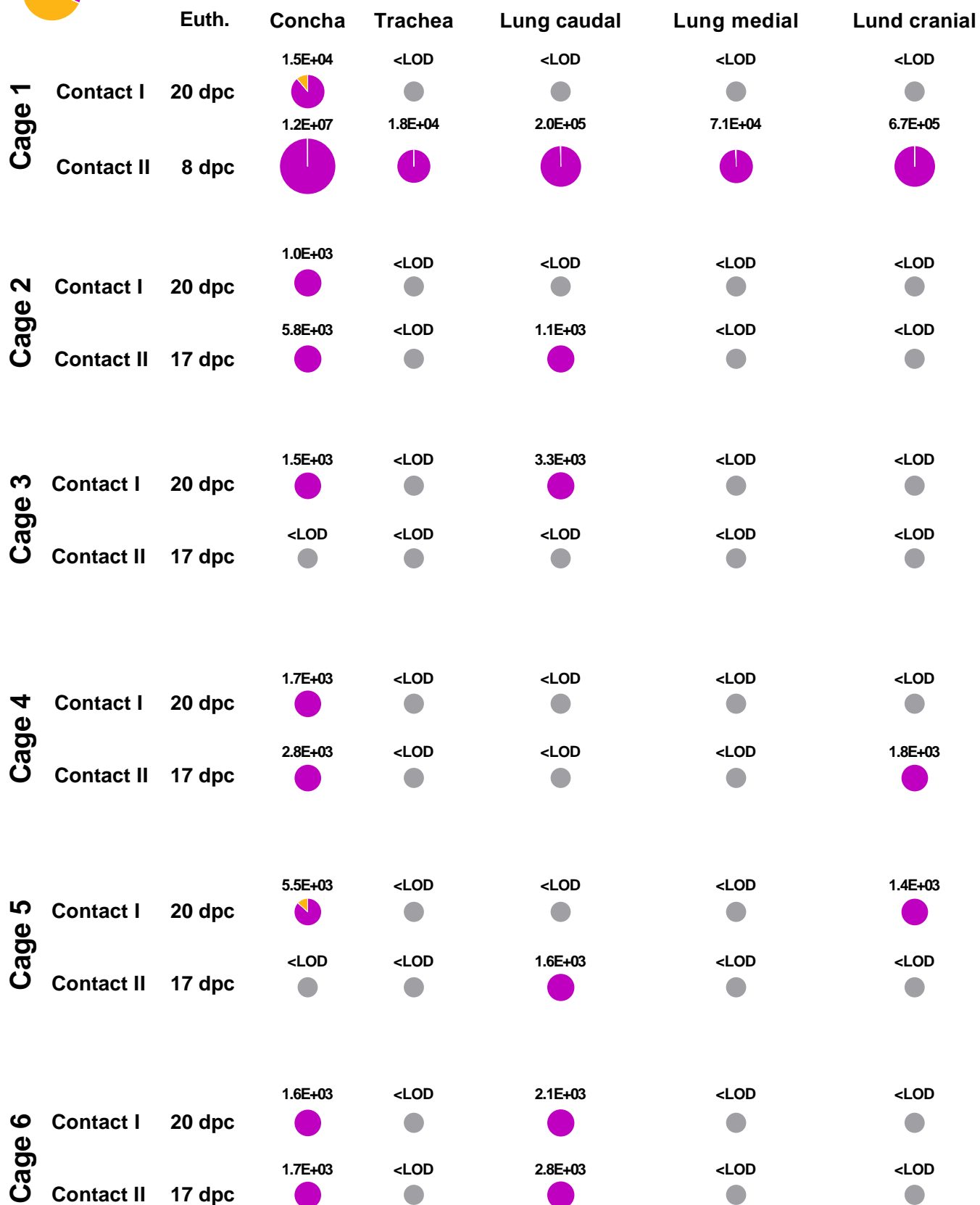


Donor
Contact

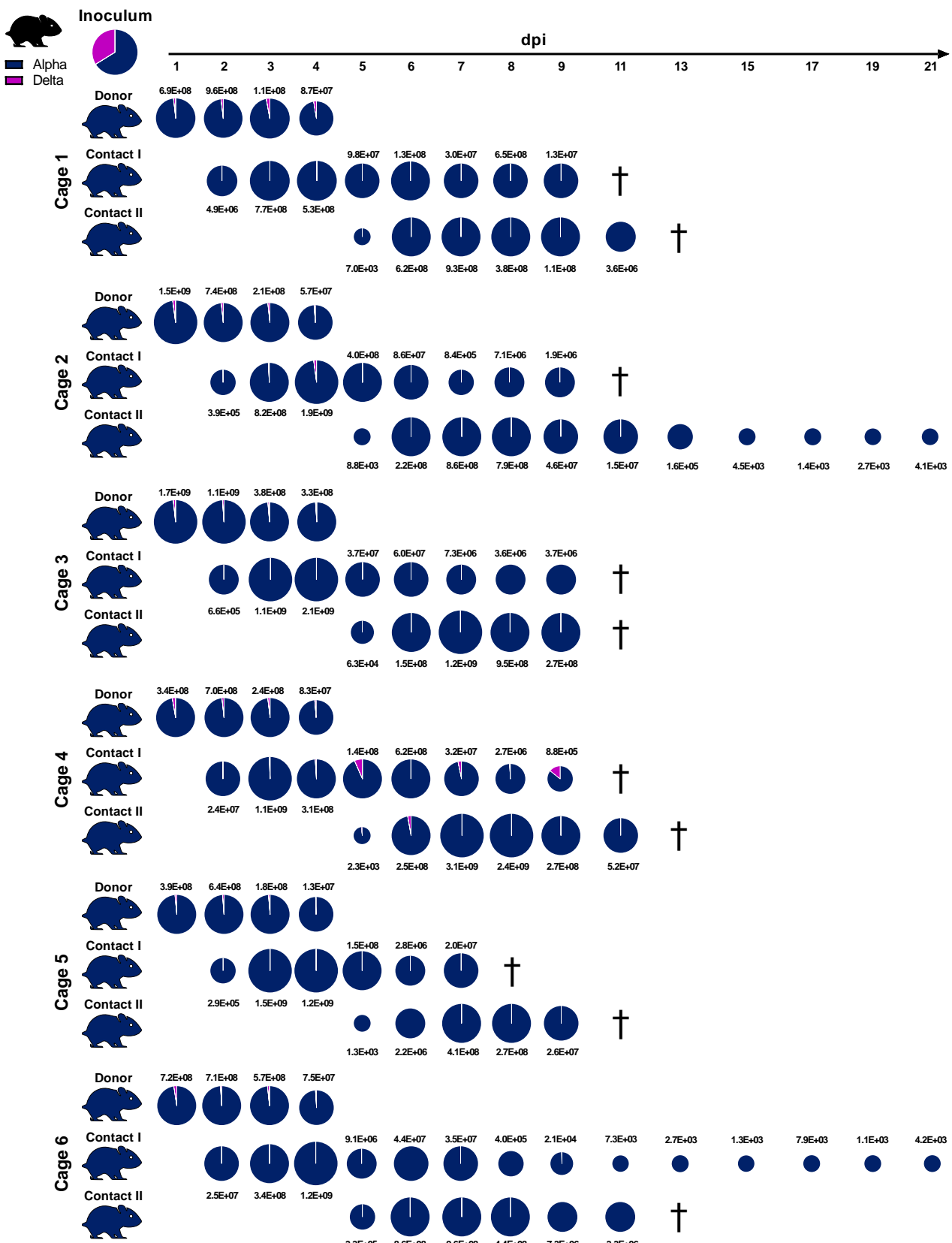


Extended Data Figure 4

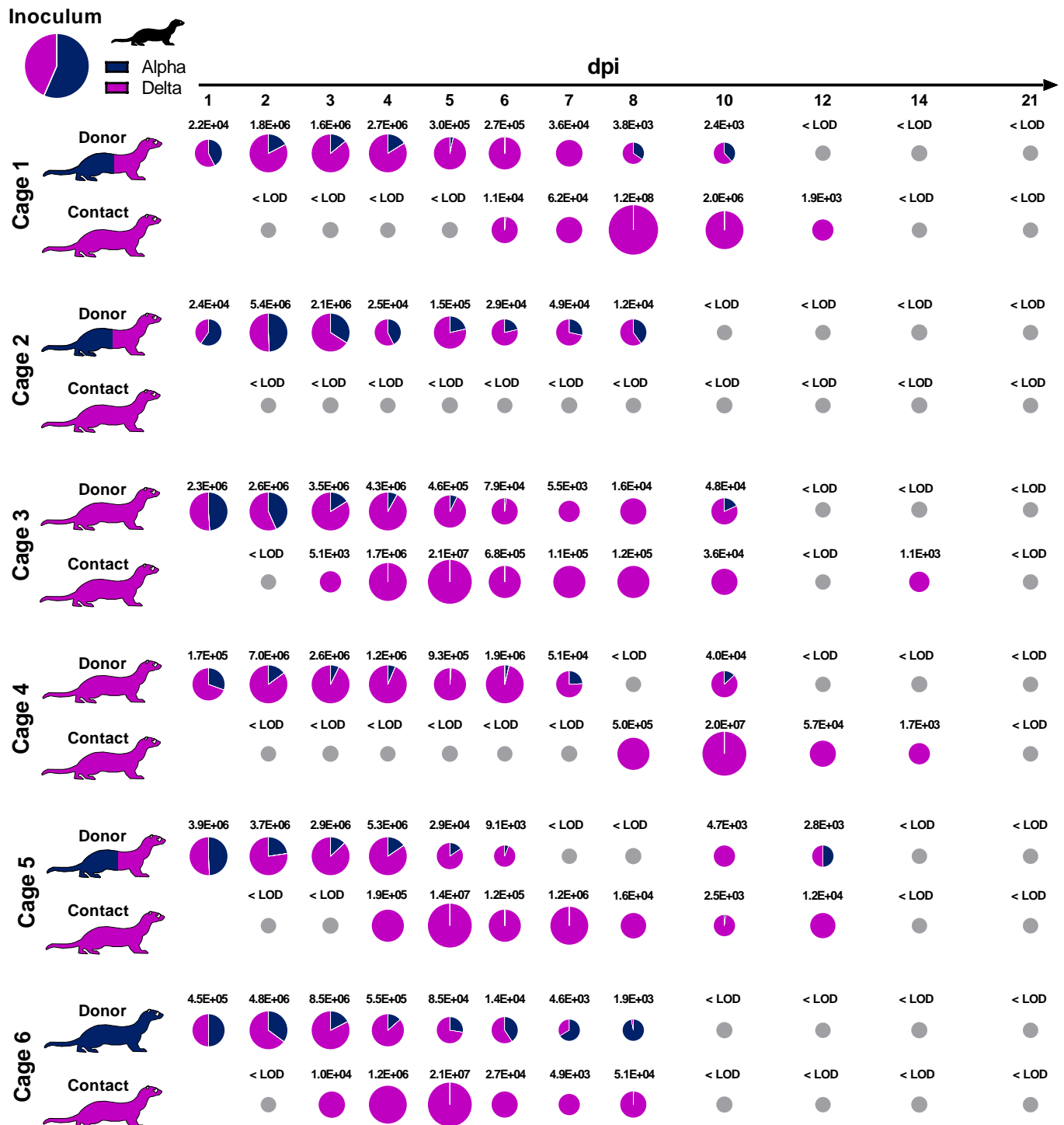
Inoculum



Extended Data Figure 5

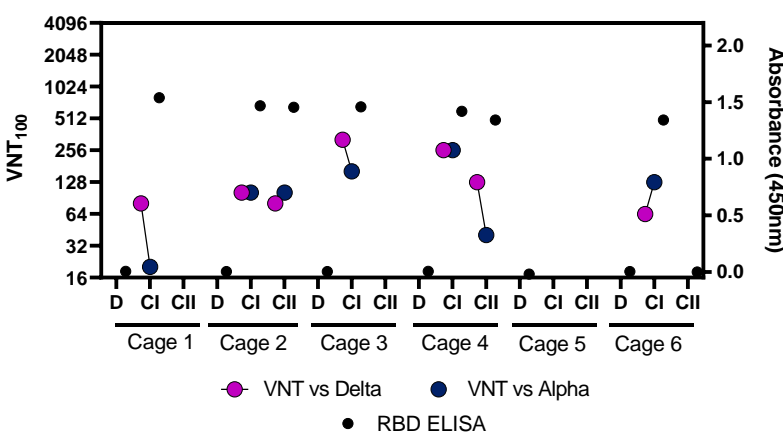


Extended Data Figure 6

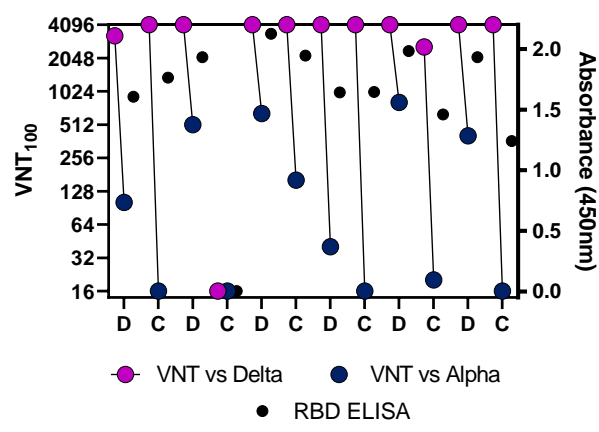


Extended Data Figure 7

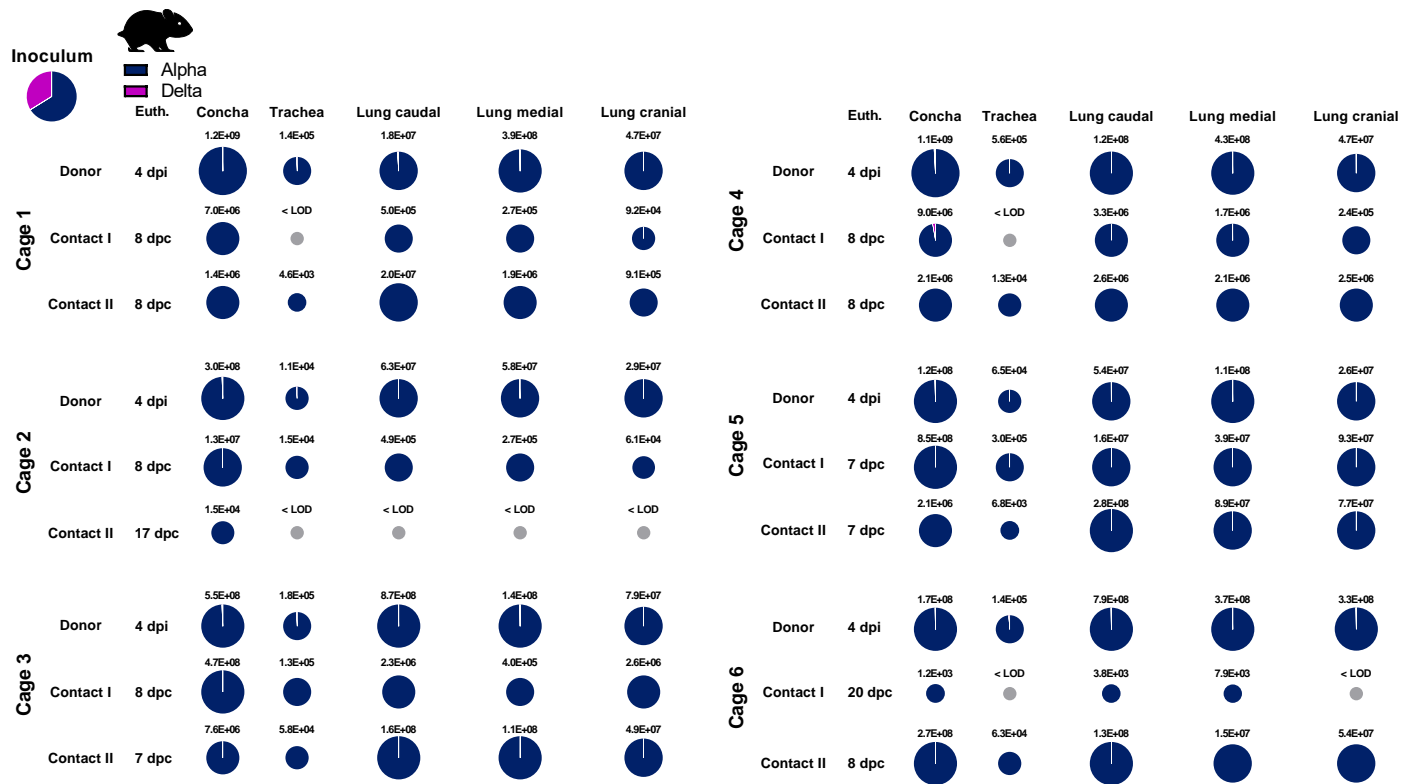
a  Alpha
Delta



b  Alpha
Delta

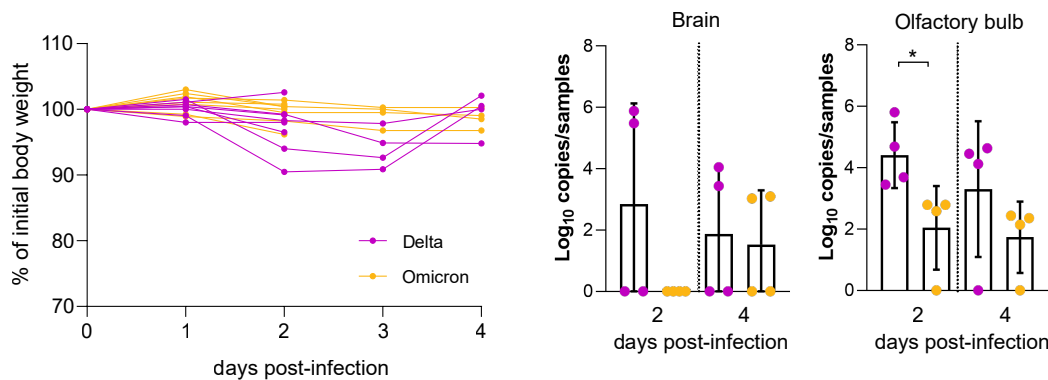


Extended Data Figure 8

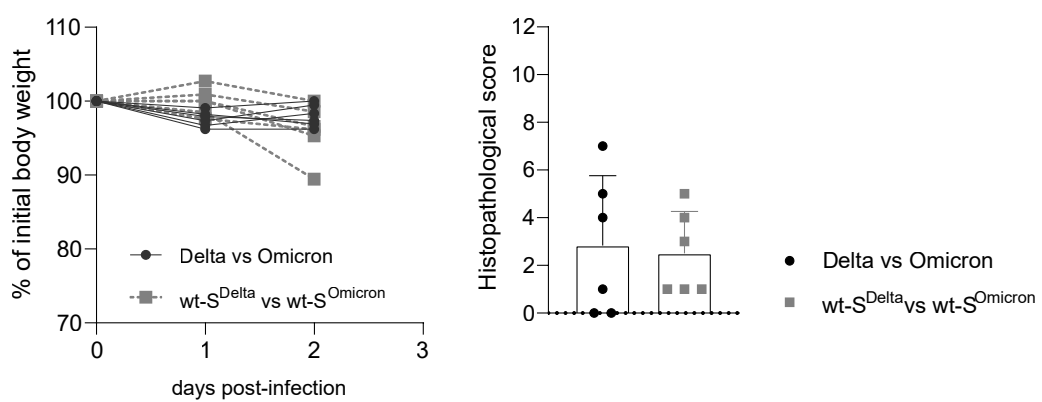


Extended Data Figure 9

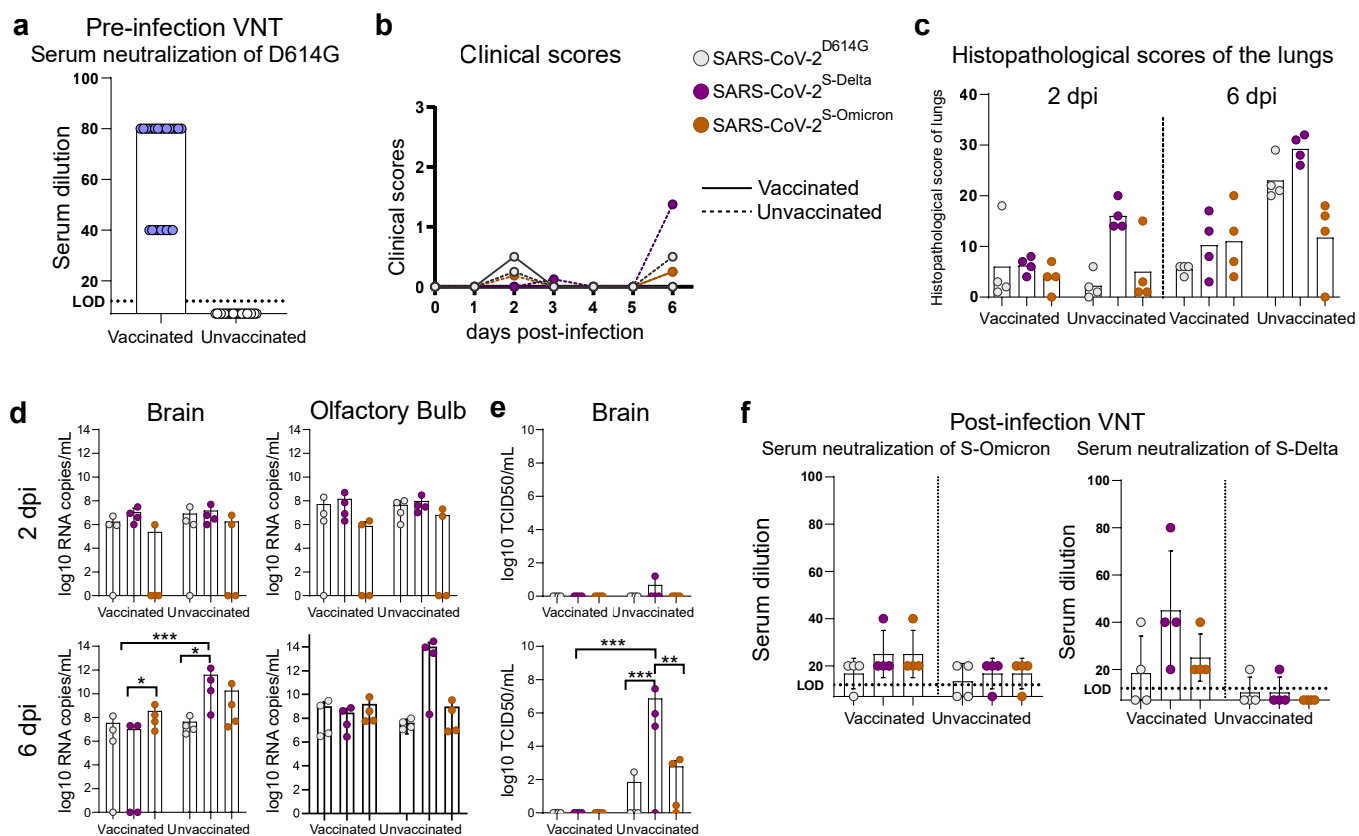
a Single infections with Delta and Omicron



b Competition experiments with Delta, Omicron, S-Delta and S-Omicron



Extended Data Figure 10



Extended Data Table 1

SARS-CoV-2	Reference	Model	Inocula
SARS-CoV-2 ^{D614G}	https://doi.org/10.1101/2022.04.28.489537	hACE2-K18 mice	SARS-CoV-2 ^{D614G} Single
			SARS-CoV-2 ^{D614G} Single
			SARS-CoV-2 ^{D614G} vs Delta
		hNEC/hBEC	SARS-CoV-2 ^{D614G} vs Omicron-BA.1
			SARS-CoV-2 ^{D614G} vs SARS-CoV-2 ^{S-Delta}
			SARS-CoV-2 ^{D614G} vs SARS-CoV-2 ^{S-Omicron}
Alpha	EPI_ISL_751799	Hamster and ferret	Alpha vs Delta
Delta	EPI_ISL_1760647	Ferret	Delta Single
			Alpha vs Delta
		Hamster and ferret	Delta vs Omicron-BA.1
			Delta Single
			SARS-CoV-2 ^{D614G} vs Delta
			Delta vs Omicron-BA.1
		hNEC/hBEC	Delta vs SARS-CoV-2 ^{S-Delta}
			Delta Single
Omicron-BA.1	EPI_ISL_6959868	hACE2-KI mice	Delta vs Omicron-BA.1
		hACE2-KI mice	Omicron-BA.1 Single
	EPI_ISL_7062525	Ferret	Delta vs Omicron-BA.1
			Omicron-BA.1 Single
		hNEC/hBEC	Delta vs Omicron-BA.1
			Omicron-BA.1 Single
SARS-CoV-2 ^{S-Delta}	Will be provided	hACE2-KI mice	SARS-CoV-2 ^{S-Delta} vs SARS-CoV-2 ^{S-Omicron}
			SARS-CoV-2 ^{S-Delta} Single
			SARS-CoV-2 ^{D614G} vs SARS-CoV-2 ^{S-Delta}
		NEC/BEC	Delta vs SARS-CoV-2 ^{S-Delta}
			SARS-CoV-2 ^{S-Delta} vs SARS-CoV-2 ^{S-Omicron}
			SARS-CoV-2 ^{S-Delta} vs SARS-CoV-2 ^{S-Omicron}
SARS-CoV-2 ^{S-Omicron}	Will be provided	PCLS	SARS-CoV-2 ^{S-Delta} vs SARS-CoV-2 ^{S-Omicron}
			SARS-CoV-2 ^{S-Delta} vs SARS-CoV-2 ^{S-Omicron}
		hACE2-KI mice	SARS-CoV-2 ^{S-Omicron} Single
			SARS-CoV-2 ^{D614G} vs SARS-CoV-2 ^{S-Omicron}
			Omicron-BA.1 vs SARS-CoV-2 ^{S-Omicron}
			SARS-CoV-2 ^{S-Delta} vs SARS-CoV-2 ^{S-Omicron}
		PCLS	SARS-CoV-2 ^{S-Delta} vs SARS-CoV-2 ^{S-Omicron}